INL/EXT-05-00306

INL Advanced Radiotherapy Research Program Annual Report 2004

Edited by J. R. Venhuizen

June 2005

The INL is a U.S. Department of Energy National Laboratory
operated by Battelle Energy Alliance

INL/EXT-05-00306

INL Advanced Radiotherapy Research Program Annual Report 2004

Edited by J. R. Venhuizen

June 2005

Idaho National Laboratory

Idaho Falls, Idaho 83415

Prepared for the
U.S. Department of Energy
Office of Science
Under DOE Idaho Operations Office
Contract DE-AC07-05ID14517

ABSTRACT

This report summarizes the activities and major accomplishments for the Idaho National Laboratory Advanced Radiotherapy Research Program for calendar year 2004. Topics covered include boron analysis in biological samples, computational dosimetry and treatment planning software development, medical neutron source development and characterization, and collaborative dosimetry studies at the RA-1 facility in Buenos Aires, Argentina.

CONTENTS

FIGURES

MINERVA RADIATION TREATMENT PLANNING SOFTWARE DEVELOPMENT

EPITHERMAL NEUTRON BEAM DEVELOPMENT FOR PRECLINICAL NEUTRON CAPTURE THERAPY RESEARCH AT WASHINGTON STATE UNIVERSITY

FIGURES (Continued)

PROGRESS ON MEASUREMENT OF TRANSPORT BENCHMARKS FOR PHYSICAL DOSIMETRY TO SUPPORT DEVELOPMENT OF FAST-NEUTRON THERAPY WITH NEUTRON CAPTURE AUGMENTATION

FIGURES (Continued)

COLLABORATIVE PHYSICAL AND BIOLOGICAL DOSIMETRY STUDIES FOR NEUTRON CAPTURE THERAPY AT THE RA-1 RESEARCH REACTOR FACILITY

TABLES

COLLABORATIVE PHYSICAL AND BIOLOGICAL DOSIMETRY STUDIES FOR NEUTRON CAPTURE THERAPY AT THE RA-1 RESEARCH REACTOR FACILITY

ACRONYMS AND ABBREVIATIONS

ANL	Argonne National Laboratory
BNCT	Boron Neutron Capture Therapy
BPA	boronated phenylalanine
BSH	borocaptate sodium
cGy	centiGray
cm	centimeter
CNEA	National Atomic Energy Commission of Argentina
CPU	central processor unit
CRADA	Cooperative Research and Development Agreement
CT	computed tomography
CY	calendar year
DOE	Department of Energy
DORT	Discrete Ordinates Radiation Transport
eV	electron volt
FiR 1	Finnish Research Reactor
FNT	fast neutron therapy
FY	fiscal year
g	gram
GB-10	$Na_2B_{10}H_{10}$
Gy	gray (absorbed dose)
GPU	graphics processing unit
HPGe	high-purity germanium
HTML	hypertext markup language
ICP-AES	inductively coupled plasma-atomic emission spectrometry
in	inch
INEEL	Idaho National Engineering and Environmental Laboratory
INL	Idaho National Laboratory
jar	Java archive file
JART	Java neutron transport code
JOGL	Java to OpenGL
JRE	Java runtime environment
keV	kilo-electron volt
kW	kilowatt
LLNL	Lawrence Livermore National Laboratory
m	meter
MCNP	Monte Carlo N-Particle
MeV	Million-electron volt
mfp	mean free path
mg	milligram
MINERVA	Modality-Inclusive Environment for Radiotherapeutic Variable Analysis

ACRONYMS AND ABBREVIATIONS (Continued)

mm	millimeter
MRI	magnetic resonance image
MSU	Montana State University
MTR	molecular targeted radiotherapy
MW	Megawatt
n	neutron
NCT	neutron capture therapy
NIST	National Institute of Standards and Technology
NIU	Northern Illinois University
NNSA	National Nuclear Energy Security Agency
NTL	Neutron Therapies, Limited Liability Company
ppm	parts per million
QA	Quality assurance
RSICC	Radiation Shielding Information Computational Center
s	second
SC	Office of Science
SERA	Simulation Environment for Radiotherapy Applications
SQL	standard query language
TLD	thermoluminescent dosimeter
TRIGA	Transient Reactor Irradiator-General Atomics
UCD	University of California, Davis
UCLA	University of California, Los Angeles
UCSF	University of California, San Franciso
UI	user interface
UT	University of Tennessee
UW	University of Washington
WSU	Washington State University
XML	extensible markup language
2D	two-dimensional
3D	three-dimensional

INL ADVANCED RADIOTHERAPY RESEARCH PROGRAM ANNUAL REPORT 2004

INTRODUCTION AND EXECUTIVE SUMMARY

The Idaho National Laboratory (INL) Advanced Radiotherapy Research Program completed its 18th year under the sponsorship of the U.S. Department of Energy (DOE), Office of Science (SC). This report includes detailed articles summarizing major INL activities and accomplishments during calendar year 2004.

As a result of various realignments over the few years, the scope of the INL program has grown beyond its original focus on neutron capture therapy (NCT) to encompass the development of enabling technologies for a significantly broader range of emerging radiotherapy modalities. The primary mission of the program, which has featured a comprehensive network of domestic and international collaborations over the last few years, is the performance of applied research and technology development to enable the application of emerging radiotherapy modalities that show promise for improved treatment of cancer and possibly other diseases. Of particular interest is a new activity focused on collaboration with The University of California at Davis (UCD), Lawrence Livermore National Laboratory (LLNL), and several other partners in the field of advanced multimodality computational dosimetry and treatment planning software development. Additional tasks involving analytical chemistry, small-animal boron agent screening studies, and development of neutron sources and benchmark dosimetry data for NCT as well as for fast-neutron therapy (FNT) also achieved significant milestones during the year.

Essentially all of the activities encompassed by the INL program are performed in close collaboration with several other institutions having similar interests. Where a benefit to the U.S. effort is realized, the INL has also maintained formal cooperative arrangements with international collaborators, specifically in The Netherlands, Finland, Sweden, Russia, and, of particular recent interest, Argentina. These collaborative arrangements have resulted in substantial leveraging of DOE-SC funding in essentially all areas of the overall INL program.

The historical INL role as a center for quantitative boron analysis and radiation treatment planning software development and deployment continued during 2004. Biological samples and boron agent samples submitted to the INL by federally supported NCT research organizations were analyzed for boron content in accordance with well-established standards, and the results were reported back to the submitting organizations. The internationally recognized INL SERA (Simulation Environment for Radiotherapy Applications) computational dosimetry and treatment planning software system continued to be supported during the year, and new national and international licensees continued to join the SERA user community. NCT and FNT research centers worldwide continue to serve as benchmarking and testing institutions for SERA, providing extremely valuable feedback and suggestions for improvement although the code has essentially stabilized in its final form at this point. A planned task during the upcoming

year involved finalizing the documentation for SERA in an externally releasable form and assembling a final validated code distribution package per applicable DOE distribution requirements. The final package will be submitted for unrestricted distribution via the DOE Radiation Shielding Information Computational Center (RSICC) at Oak Ridge National Laboratory. The SERA Internet site will be actively maintained through FY 2005, with a referral to RSICC for distribution thereafter. This will complete the SERA treatment planning development project, which has been supported by DOE-SC since 1996.

With the completion of SERA, the developmental focus is now on the new MINERVA (Modality Inclusive Environment for Radiotherapeutic Variable Analysis) multimodality radiotherapy computational dosimetry treatment planning system. This effort involves a broad collaboration as noted above. This project takes advantage of the many benefits of using the Java programming language to create a "next-generation" modality independent system for a wide variety of research applications in essentially all traditional and emerging fields of radiotherapy.

INL also continued its efforts toward the development and benchmarking of neutron sources useful for NCT, FNT, and NCT-augmented FNT. This has involved collaborations with the University of Washington (UW) fast-neutron radiotherapy program, the Washington State University (WSU) Nuclear Radiation Center and School of Veterinary Medicine, the University of Essen (Germany) and, of particular interest during the past year, the neutron radiotherapy program at the Fermi National Accelerator Laboratory. This effort has a focus on providing high-quality benchmark data for validation of advanced 3D Monte Carlo based treatment planning systems, such as SERA and MINERVA, as well as others under development elsewhere. In addition, construction of a new epithermal neutron beam facility for preclinical research at WSU was completed during the year, with the first demonstration of the thermalized beam capability in November. Final characterization of both the thermal and epithermal beams per the currently emerging international standard will be conducted during 2005.

Finally, in addition to the domestic NCT activities supported at the INL by DOE-SC, INL researchers continued a very fruitful collaboration with the National Atomic Energy Commission of Argentina (CNEA) in the areas of NCT beam dosimetry and small-animal radiobiology. This collaboration is partially supported by the DOE National Nuclear Energy Security Agency (NNSA) with additional in-kind contributions from an INL CRADA (Cooperative Research and Development Agreement) partner, Neutron Therapies, LLC.

BASELINE CHEMISTRY SUPPORT

W.L. Bauer[1], B.M. White[1]

1. Idaho National Laboratory, Idaho Falls, ID

DETERMINATION OF BORON IN BIOLOGICAL SAMPLES

During calendar year (CY) 2004, 180 new samples were received for analysis by inductively coupled plasma atomic emission spectroscopy (ICP-AES) using standardized procedures established by INL scientists. With additional Quality Assurance (QA) samples, the total number of samples analyzed came to 211. Of the samples received, 25 were from dogs and/or rodents from Boron Neutron Capture Therapy and related programs in Dr. P. Gavin's group at Washington State University (WSU), 26 were of stock solutions to be sent to WSU and assorted other preparations from Dr. F. Hawthorne's group at University of California, Los Angeles (UCLA), and 129 were from the University of California, San Francisco (UCSF). During CY 2005, a few samples are expected from UCLA and from UCSF. ICP capabilities are now available at WSU to support their local program, and only verification samples will be analyzed for them.

MINERVA RADIATION TREATMENT PLANNING SOFTWARE DEVELOPMENT

D.E. Wessol[1,2], C.A. Wemple[1], D.W. Nigg[1], J.J. Cogliati[1], M.L. Milvich[1], C.M. Frederickson[2], M.Y. Perkins[2], D.K. Lyle[3], C.D. Frederickson[2]

1. Idaho National Laboratory, Idaho Falls, ID
2. Montana State University, Bozeman, MT
3. BP Center for Visualization, University of Colorado, Boulder, CO

INTRODUCTION

Development of the MINERVA (Modality-Inclusive Environment for Radiotherapeutic Variable Analysis) general purpose treatment planning system continued at Montana State University (MSU). Efforts focused on making the software, which is written entirely in the Java programming language (Gosling 1996), more robust, more adaptable to new hardware and software technologies, and easier to install on various computers. Improved patient data management, internal code documentation and help system, improved code configuration and management, and unit testing features were added to MINERVA. Support was also extended to Windows XP. The development of a high-speed, three-dimensional, neutron transport plugin is currently under development at Idaho National Laboratory (INL), and a deformable registration method is being developed at the BP Center for Visualization at the University of Colorado. The Patient, Image, Model, and Analyze modules are also undergoing improvement.

DATA MANAGEMENT

While the goals of the data management system have not changed over the past year, the implementation is completely new. The new implementation offers several advantages:

- The persistence layer is now multi-threaded, allowing multiple modules to use the data system simultaneously. For example, while waiting for the geometry to load, the user can edit and save an image set. The data to be persisted is defined using Java's metadata[a] facility on a per object basis. Each object defines which fields should be persisted, along with the type of the field and other special parameters that may be needed.
- The hibernate[b] object-relational mapper is used to generate the standard query language (SQL) (ANSI X3.135, 1992) needed to communicate with the database based on the information provided by the object's metadata. Hibernate also abstracts the subtle differences between databases into database dialect classes. This will allow many database engines to be easily supported by simply changing the dialect being used.
- The database schema has been greatly simplified. Previously, the number of tables in the database grew every time new objects were created for a patient. After several patients had been stored, the number of tables was unmanageable. Objects of the same type are now stored together, which allows the number of tables to remain fixed after installation.

[a] Java metadata: http://jcp.org/en/jsr/detail?id=175
[b] hibernate: http://hibernate.org

- The extensible markup language (XML)[c] part of the persistence system is also being re-factored to use the defined metadata. By using the same metadata for all data persisters, a change to the metadata will cascade and allow all persisters to remain in-sync. This frees developers from maintaining cross-data source compatibility by hand.
- The impact of adding a new data source to the system has been greatly reduced. Adding a new data source consists of (a) implementing an interface to define how the data maps onto the data source and (b) providing hooks for the new persister into the system.

HELP SYSTEM

A help system was developed for MINERVA. This system provides an intuitive help information facility that allows users to navigate, search, and display help information, as shown in Figure 1. It can also help users learn how to use the system, reducing the initial training time.

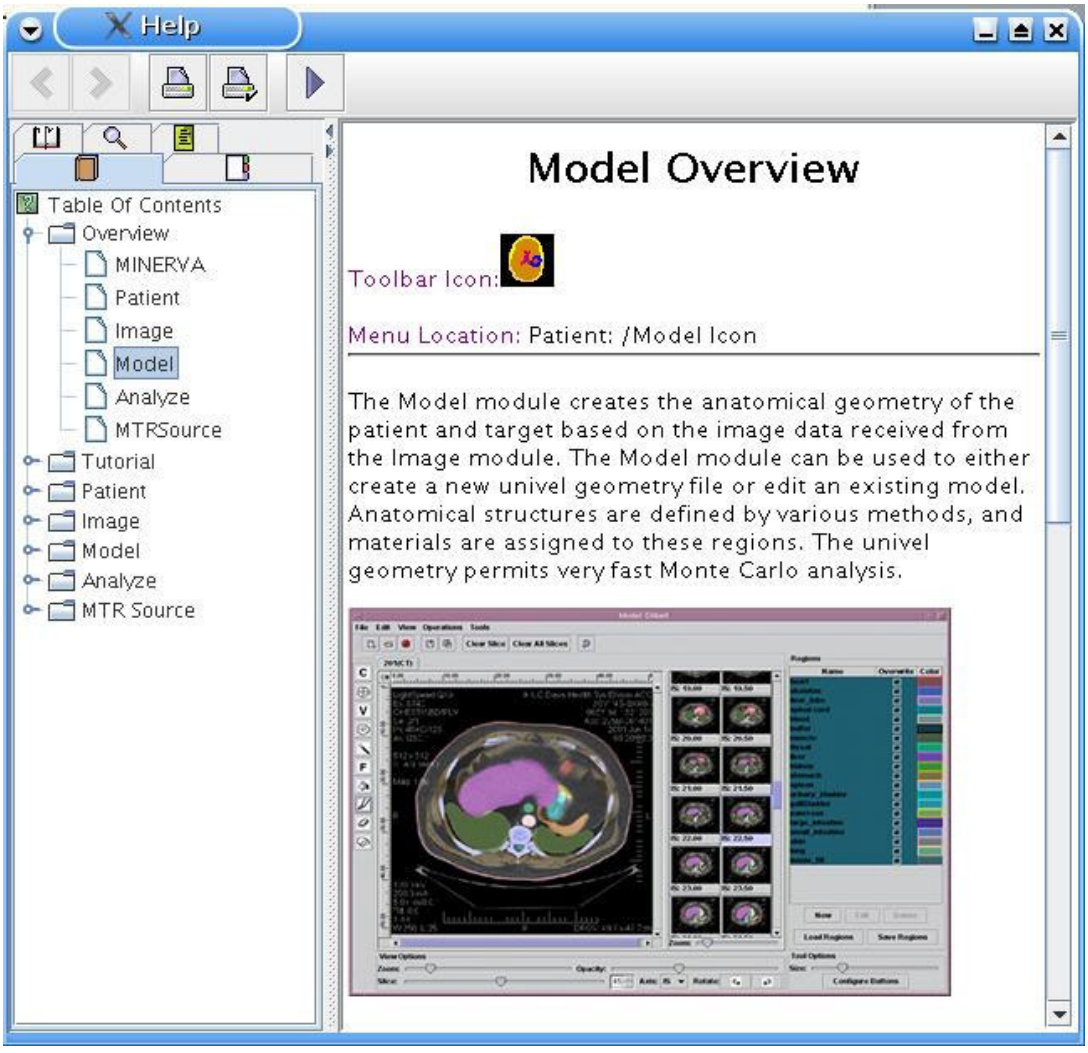

Figure 1. The MINERVA help system.

[c] Coding of multimedia and hypermedia information-Part 8: XML notation for ISO/IEC 13522-5.

The JavaHelp (Lewis 2000) extensions were used. JavaHelp is an extensible, platform-independent help system that enables authors and developers to incorporate online help into applets, applications, operating systems, and devices. The content pages are hyper-text markup language (HTML) documents and contain text, links, and images.

The help system contains information about MINERVA, each of the modules, and the molecular targeted therapy (MTR) plugin. The help system has a table of contents with a tree structure displaying all the pages, an index, a glossary of terms, and a search function. Information for additional plugins can be added as needed, as can tutorials. Currently, the help system can be launched from any one of the MINERVA modules or plugins. The system can also be made available online.

INSTALL SYSTEM

As the configuration of MINERVA utilizes more and new technologies, the installation procedure becomes more complex. MINERVA itself can be run on any machine with version 1.5 of the Java runtime environment (JRE). The JRE distributed by Sun[d] is platform dependent, so a user must first download and install the appropriate JRE before using the program. The various Java technologies employed by MINERVA require the installation of Java archive (jar) files in the appropriate operating system dependent location on the user's file system.

An install wizard is being developed to facilitate the install process. Several commercial products are being evaluated. Zero G[e] produces the "Install Anywhere" wizard. This can be customized to our installation requirements, and will control the JRE used to run the program. An installer will be provided for both users and developers. The developer version of the installer will contain the interface documentation to build new plugins.

CODE CONFIGURATION AND MANAGEMENT

Up to this point, MINERVA and neutron transport model development have been done using CVS[f] as the versioning system. CVS keeps track of old versions of the software and merges changes made by different developers, which makes group development easier. However, CVS does not provide a way to move a file or a directory while keeping the change history with the moved file. Since the MINERVA directory structure was going to be reorganized, the history would have become more difficult to access under CVS. CVS allows finding the history only by knowing the original directory and name, since as far as CVS is concerned, the old directory or file and the new one are completely independent. The impending directory reorganization provided the motivation to move to a new versioning system, Subversion[g]. Subversion is being developed as a CVS replacement, so it has most of the CVS features as well as new features. In addition, the tool cvs2svn converts CVS repositories to Subversion repositories without losing change history. For MINERVA development, the most important improvement in Subversion is the ability to track changes as files and directories are moved, which was used in the directory reorganization after the Subversion switch occurred.

---

[d] Sun Microsystems Inc., Sunnyvale, CA
[e] Zero G Software, Inc. San Francisco, CA
[f] Concurrent Version Systems, freeware
[g] For Example: Version Control with Subversion, C. Michael Pilato, B, et al., 2004, O'Reilly

CODE FORMATTING

The Jalopy[h] Java formatting tool is being used with the MINERVA source code. This tool will increase the readability and maintainability of the source code by creating a uniform format throughout the source code. In addition, the code formatting allows Javadoc comments to be generated automatically for classes and methods that have previously been undocumented. This will allow new developers on the project to more easily gain an understanding of the project, as well as showing current developers the functionality of all the different pieces of the project. Jalopy is invoked using the MINERVA build script to ensure that all code is formatted. It also integrates with the Eclipse[i] and Netbeans[j] integrated development environments that are being used by the majority of the MINERVA developers.

Jalopy has much more flexibility than the formatting tools built into various integrated development environments, which allows everyone to use the same code formatter regardless of their environment preference. Jalopy is also the only code formatter that supports all the Java 5.0 constructs, which is crucial since a majority of the new code is written using 5.0 constructs. Another feature of the formatter is that it contains the ability to enforce the "Effective Java" rules. These rules have been published by Sun Microsystems and should be followed in order to write the most effective source code.

UNIT TESTING

In order to improve software quality, provide accurate documentation, and improve design in the software, unit tests[k] are being added to a unit test directory in the main trunk of the repository. The structure of the test directory exactly mirrors that of the Minerva source directory. Tests for classes in a specific source directory should be placed in the corresponding test directory. For example, if a test is written for the class *minerva.tirade.patient.PatientUI,* it should be placed in the *test.tirade.patient* package.

Unit testing allows small pieces of a system to be tested independently. Base tests typically test a single class, while other tests use the base tests together to test larger chunks of related code. This process can be repeated until whole subsystems or the entire system is being tested together. If a problem arises after code changes are made, locating the problem should be relatively easy and should quickly narrow the error to a specific base test. This assumes that a sufficient number of tests have been written for the system.

The testing is actually done by JUnit[l] - a framework to assist developers in writing repeatable tests. Writing a unit test is as simple as extending the JUnit TestCase class. To define a test case:

1) implement a subclass of TestCase
2) define instance variables that store the state of the fixture

---

[h] http://www.triemax.com/products/jalopy/manual/
[i] http://www.eclispe.org
[j] Netbeans is a Trademark of Sun Microsystems (http://www.netbeans.org)
[k] http://www.onjava.com/pub/a/onjava/2003/04/02/javaxpckbk.html
[l] http://junit.sourceforge.net

3) initialize the fixture state by overriding setUp
4) clean-up after a test by overriding tearDown.

Each test runs in its own fixture so there can be no side effects among test runs. An example from the JUnit documentation follows:

```
public class MathTest extends TestCase
{
   protected double fValue1;
   protected double fValue2;

   protected void setUp()
   {
      fValue1= 2.0;
      fValue2= 3.0;
   }
```

For each test, implement a method that interacts with the fixture. Verify the expected results with assertions specified by calling assertTrue with a boolean.

```
   public void testAdd()
   {
      double result= fValue1 + fValue2;
      assertTrue(result == 5.0);
   }
}
```

The tests have also been integrated into the Ant[m] build file, so they can easily be run at any time. Ideally, a developer will test the subsystem as changes are made, and then run the entire test suite before committing the changes back to the main development trunk.

DEFORMABLE REGISTRATION

The multimodal rigid image registration functionality in MINERVA is being extended to perform non-rigid image registration. Initial steps included implementing a three-dimensional (3D) volume viewer that will display both the reference and deformed image sets simultaneously. The 3D viewer was implemented using OpenGL[n] replacing the existing, primitive, Java3D based viewer in the registration module. The 3D viewer will be the primary view of the image sets in the registration module with side-by-side 2D slice displays also included. The motivation for this decision was the inherent difficulty in interpreting 3D alignment from 2D slices. Work has also been completed to automatically partition large volumes into smaller sub-volumes, allowing the display of arbitrarily large volumes independent of the amount of memory on the graphics hardware. The new 3D display also provides the basis for the calculation engine for the non-rigid registration algorithm.

Several methods have been proposed to perform deformable, non-rigid registration. Early non-rigid registration approaches used linear elasticity models (Christensen 1994,

[m] http://access1.sun.com/techarticles/Ant.html
[n] http://www.opengl.org

Gee 1993, Evans 1991, Bajcsy 1989). The elasticity models enforce global smoothness in the deformations and thus only allow small deformations. Christensen (Christensen 1996) then detailed the use of a partial differential equation based viscous fluid model to control the deformations. The test image is a viscous fluid that flows to match the reference image. Internal forces drive the deformations, and eventually those forces subside due to the attenuation of viscous fluids. The viscous fluid model allows large deformations while preserving topology. The drawback of this model is that it is computationally expensive.

In an attempt to improve performance, the fluid flow modeling will be performed on the graphics processing unit (GPU) rather than the central processing unit (CPU) (Kruger 2003, Lefohn 2003, Larsen 2001, Rumpf 2001, Strzodka 2001). The GPU provides a parallel, single instruction, multiple data processor to perform floating point calculations. The GPU has more bandwidth from the memory than the CPU, allowing the GPU to read data faster than the CPU. Programming for the GPU is being accomplished using OpenGL Shading Language[o], a part of the OpenGL specification. An additional advantage to using the GPU to perform the registration algorithm is that the user will get visual progress updates as work is performed without additional computational expense.

Currently a proof of concept has been implemented which performs all image processing in the 3D viewer on the GPU with a marked performance improvement. Implementation of the fluid flow model is currently under way with preliminary results expected in late FY 2005.

NEUTRON TRANSPORT MODULE (JART)

A univel geometry, neutral particle Monte Carlo transport code, written entirely in the Java programming language, is under development for medical radiotherapy applications. The code uses ENDF-VI[p] based continuous energy cross section data in a flexible XML format. Full neutron-photon coupling, including detailed photon production and photonuclear reactions, is included. Charged particle equilibrium is assumed within the patient model so that detailed transport of electrons produced by photon interactions may be neglected. External beam and distributed internal source descriptions for mixed neutron-photon sources are allowed. Flux and dose tallies are performed on a univel basis. A four-tap, shift-register-sequence random number generator (Ziff 1998) is used.

The solution space defined in the input is subdivided into univels, which are rectangular parallelepipeds of uniform size. The transport method uses a three-dimensional variation (Frandsen 2001, 1998a, 1998b) of Bresenham's line drawing algorithm (Bresenham 1965) for the ray tracing and particle tracking. Enhancements to the algorithm were made to incorporate an improved method for calculating the total distance traveled across each univel, which is a necessary quantity for calculating tallies on a univel basis.

The univel particle tracking algorithm is initialized with a location and a direction for each particle. This initialization occurs at the birth of a particle and at each collision.

---

[o] http://www.opengl.org/documentation/oglsl.html

[p] Evaluated Nuclear Data File, compiled and maintained by the National Nuclear Data Center (NNDC) at the Brookhaven National Laboratory (http://www.nndc.bnl.gov/exfor/endf00.htm)

The distance to collision is sampled in the normal fashion. At each univel boundary crossing, a check is performed to see if a new material is encountered; if so, a new distance to collision is sampled. Because of the uniform nature of the univels, the distance traversed between boundary crossings along each spatial coordinate axis is a constant and can be calculated from the initialization values and the univel dimensions. This allows the use of (mostly) integer arithmetic to perform the particle tracking through the univels. Univel material properties can be stored in an array and accessed quickly.

The tally calculation uses a basic track length estimator, which requires the distance traveled through each univel. This distance is calculated during the univel particle tracking. As noted above, the same distance is traveled between each parallel boundary crossing along a given line. For example, each time a boundary is crossed along the x-direction, the distance that has been traveled since the previous boundary crossing in this direction can be calculated. The distance traveled in each univel is determined by knowing that each time a particle crosses a univel boundary, it has traveled a known, constant distance. This distance and a total distance are stored for each dimension, along with an overall total distance. The overall total distance is the distance at the last boundary crossing and is updated at each boundary crossing.

A two-dimensional example of this procedure is shown in Figure 2. The incremental distance in the x-direction is denoted as Dx, and as Dy in the y-direction. For the following example, let the total distance traveled at each x-direction boundary crossing be denoted as X and the total distance traveled at each y-direction crossing as Y. The total distance traveled can then be calculated by adding the incremental distance traveled to the last total distance for that dimension. Thus, the total distance traveled at point B is Dx added to the total distance X traveled at point A. When the particle reaches point C, the distance Dy is added to the last Y total distance. When point D is reached, Dx is added to the last calculated value of X, which was the total distance at point B. The same process occurs for each of the directions. The distance traveled in each univel is the difference between the total distance for the dimensional boundary crossed and the overall total distance. The particle tracking ceases when the weight reaches a user-defined cutoff or the edge of the univel space is reached.

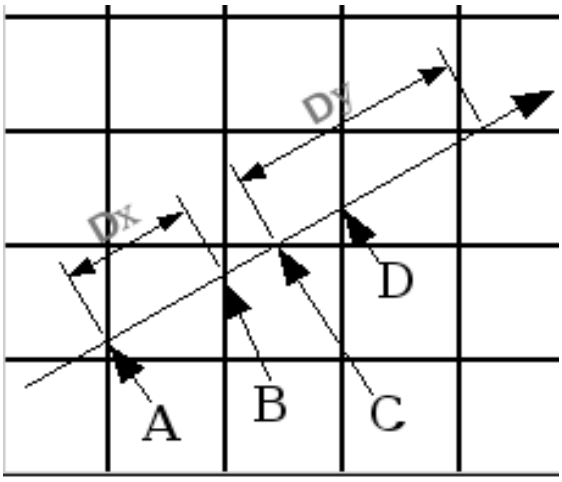

Figure 2. A two-dimensional example of ray tracing through the univel geometry.

The tallies are calculated on the univel grid defined by the problem geometry or an integer multiple of this univel grid. A standard track length estimator is used for the tallies, i.e., each time a particle passes through a univel, the distance that the particle travels times the weight of that particle is added to the tally in the univel. Tally values at a point are calculated by quadratic interpolation along the three coordinate axes, assuming that the value for a univel applies at the centroid of the univel volume. This interpolation uses the tally values for the univel containing the point and the 26 surrounding univels in 3-space.

The tally statistics estimate the deviation of the calculated tally results from the "true" results, those derived from an infinitely long calculation. It should be noted that this is not necessarily how close the answer is to the correct answer, since there are biases in the data and methods used. There are two extreme ways of calculating the "true" result. The first is to treat each particle tracked as a single experiment. The second is to treat the entire run of particles as one experiment. The first method requires statistics computation for each particle that is tracked. For the first method, the transport code was spending far more time calculating the statistics than performing the particle tracking. The second extreme does not give any idea about the precision of the calculation, since the variance of a single experiment cannot be calculated. The method used in JART allows the user to define the balance between the frequency of statistical value computation and overall calculation speed.

The searchlight problem is a classical two-dimensional radiation transport problem originally proposed by Chandrasekhar (Chandrasekhar 1958). The problem as considered for this work consists of a homogeneous half-space of material illuminated by a pencil beam of mono-energetic neutrons normal to the free surface. The solution assumes no energy dependence of the cross section and only isotropic elastic scattering. The composition of the half-space is a material with unit total cross section (99% scattering and 1% absorbing). This provides an excellent problem for testing the basic mechanics of the Monte Carlo transport, especially the tracking and tally routines.

The reference solution for this work is the analytical solution derived by Ganapol (Ganapol 1994). Computations were performed for the radial dependence of the flux at several penetration depths within the half-space. The JART model approximated the half-space by a rectangular parallelepiped of size 36x36x38 mean free paths (mfp), which adequately represents an infinite half-space. The univel size used for the calculation was 0.1x0.1x0.1 mfp. The flux as a function of radius was calculated at several different penetration depths. The JART tallies at each radial point were averaged over the four points in the primary compass directions to exploit the natural symmetry of the problem, while the MCNP (Briesmeister 2000) tallies used annular shells for surface (type 2) tallies.

The results of the JART calculations, along with the reference solution and an equivalent MCNP calculation, are shown in Figure 3. The tally statistics on the JART and MCNP results are too small to be resolved on the images. Agreement between the various methods is excellent and within the calculated tally statistics of the Monte Carlo results. This provides verification for the correct functioning of the basic transport mechanics of the JART code.

The results displayed in Figure 3 required simulation of 32×10^6 particle histories. The CPU time consumed by the JART calculation was 291 minutes, compared with 161 minutes for the MCNP calculation. Both simulations were run on a single processor Sun Blade 2000 workstation. The ratio of the computation times of JART and MCNP, which is less than a factor of two, shows that Java has the capability to perform complex scientific calculations without an undue penalty in computation time. Because of the nature of the univel geometry, increased complexity in the problem geometry will have minimal effect on the JART runtimes, but can greatly increase the runtime for MCNP. It is possible that JART could have an advantage in computation time over MCNP for clinical radiotherapy calculations. This will be verified in future investigations.

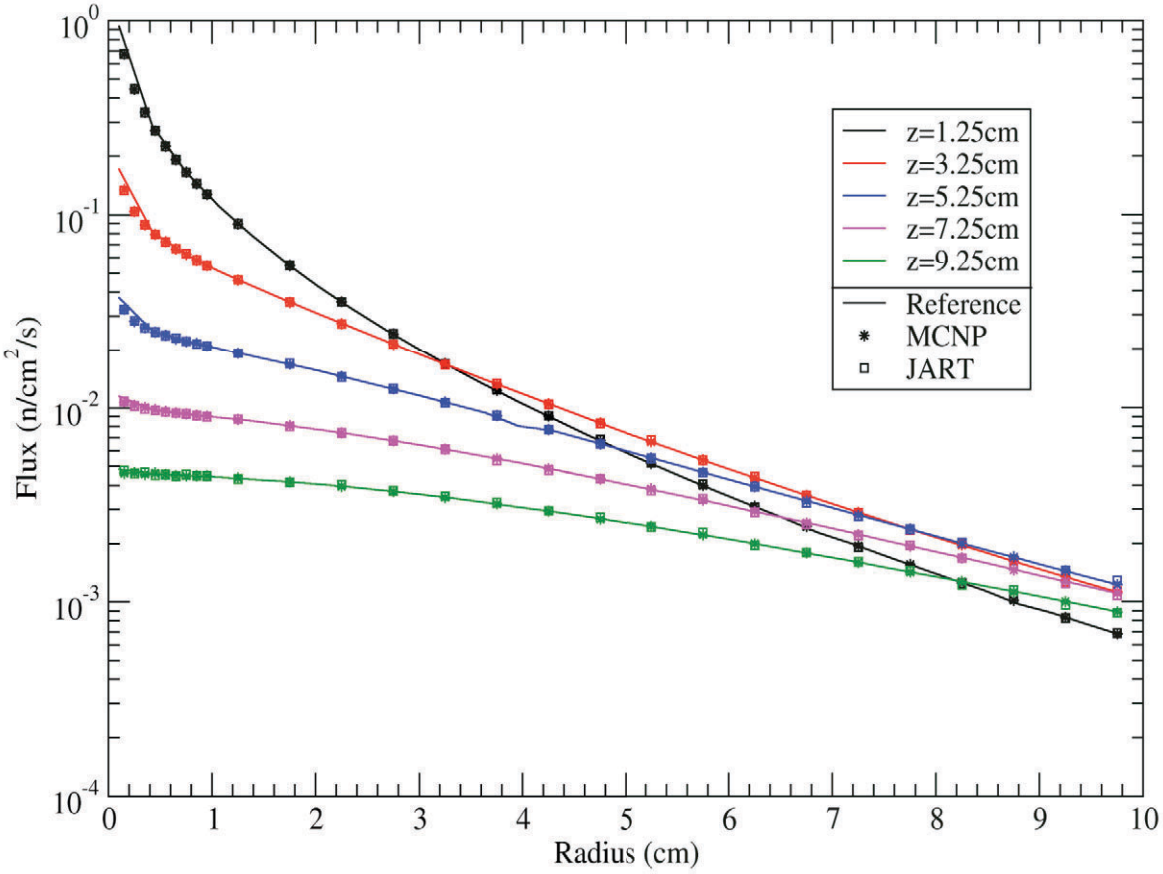

Figure 3. Comparison of searchlight problem results for several penetration depths.

JAVACAVE

A framework was created to support 3D immersive environments such as an environment provided by a CAVE®[q] or a head mounted display. Immersive environments typically use stereo projection to create lifelike 3D objects, and surround the user in a virtual world. The CAVE system surrounds the user by projecting the virtual world onto the walls and floor of a small room, while the head mounted displays place small screens right in front of the user's eyes and restricts the user from viewing the outside world.

[q] CAVE is a registered Trademark. See: http://www.evl.uic.edu/pape/CAVE/

JavaCAVE is unique in that it is written almost entirely in Java using the JOGL[r] (Java to OpenGL) library. It has a plugin system to abstract interfacing with input devices and the process of synchronizing frame updates over multiple projectors. A CAVE system typically has a projector for each wall. In order to provide a smooth, image each projector has to synchronize its refresh rates and swap the frame buffers at the same time.

JavaCAVE has been designed to work on clusters, where each machine in a cluster is responsible for one wall. Clusters make sense, since it is less expensive to buy fast PCs with good video cards then to buy a single visualization server. Of course, it is more difficult to synchronize the video cards in multiple computers to use the same refresh rate and swap buffers at the same time. Video card manufactures, such as NVIDIA[s], have graphic cards that can be networked together and configured to synchronize themselves. JavaCAVE comes with a plugin to properly configure the NVIDIA synchronization system.

Currently, JavaCAVE is able to display the geometries created in the Model module, and allows the user to point at regions and change the opacity. Work is being done to integrate and to display more information, such as the dose contours.

PATIENT MODULE

The patient module was updated to allow the user to associate a picture with a patient. In addition, a new memory window was added to monitor the memory usage and give the user more control over the Java garbage collector.

IMAGE MODULE

Most of the Image Module has been rewritten to be faster, more reliable, and have a smaller memory footprint. User responsiveness has been increased by multithreading most of the long image operations, thus allowing the user to use other modules while the Image module is busy. Progress monitors with a cancel option are now displayed for all actions requiring a noticeable delay. A drag and drop system was implemented that allows the user to reorder the images by dragging them around the Image workspace, and the user can build composite image sets by dragging images from one set into another set. An improved undo system was also developed that records only the actions needed to revert the user's actions. For example, the action required to undo a horizontal flip is a horizontal flip. The old undo system worked by saving the old data, which uses much more memory than the new system.

The restriction that all images must be 15 bits has been lifted, allowing any image from 1 to 15 bits to be used. If an image is 16 bits, then it is scaled down to 15 bits to avoid any potential problems. The image is down-sampled because Java does not support unsigned data types. Without unsigned data types, comparisons with 16 bit values become problematic, since any value over 32,767 will wrap around and become negative.

Adjustment plugins, which allow the user to modify the image color table, were added. This allows the user to change the brightness, contrast, and gamma of an image set

[r] https://jogl.dev.java.net/

[s] NVIDIA, Santa Clara CA., www.nvidia.co.uk

without changing any of the data, since the color table translates the data into the color displayed on the screen.

The DICOM[t] importer has been improved to be more generic and more reliable allowing the user to import more images then before, even if the images do not exactly follow the DICOM specification. Currently, the importer can only import magnetic resonance images (MRI), computed tomography (CT) images, and X-ray images, but it is generic enough that it can be extended to import geometries and doses.

MODEL MODULE

The user interface for the Model module has been updated by adding rulers to the main editing view and by displaying axis information. The rulers can be switched between English and metric units, and updated depending on the zoom, rotation, and the axis the user is viewing. The axis graphic also tracks any changes to rotation. In addition, a new pixel information window was created that provides information about the pixel, such as region number, name, material name, and location under the user's cursor. In order to identify undefined pixels, a command was added to jump to the next slice with an undefined pixel. The user can also change the color of undefined pixels from transparent to any other color. Finally, the tool plugins can now specify what category they belong to, and the user interface will visually group them. This displays tools, like the marker tools, together on the user interface.

ANALYZE MODULE

Most of the changes to the Analyze module have been bug fixes, but there are a few notable changes. A binary agent editor was added to allow the user to specify and configure the binary agents before the transport simulations are run. Database access has been multi threaded to allow the user to work in other modules while the Analyze module is loading the data. The Contours plugin has been updated to display the markers added in the Model module.

MTR SOURCE

The MTR Source plugin has been updated with a greatly enhanced user interface. A wizard now guides the user through a series of steps to make sure that required actions are performed at the proper times. User entered data is now checked to make sure it is valid before trying to use it. More error checking has been added when loading data from the database, and, if the database is missing some information, default values are used.

REFERENCES

ANSI X3.135, 1992, "Database Language SQL."

Bajcsy, R., Kovacic, S., 1989, "Multi-resolution elastic matching," *Computer Vision, Graphics, and Image Processing*, Vol. 46, pp. 1-21.

Briesmeister, J.F., 2000, *MCNP – A General Monte Carlo Code for Neutron and Photon Transport, Version 4C,* LA-13709-M, Los Alamos National Laboratory.

[t] DICOM: Digital Imaging and Communications in Medicine, http://medical.nema.org

Bresenham, J.E., 1965, "Algorithm for Computer Control of a Digital Plotter," *IBM System Journal*, 4, pp. 25-30.

Chandrasekhar, S., 1958, "On the Diffuse Reflection of a Pencil of Radiation by a Plane-Parallel Atmosphere," *Proceedings of the National Academy of Sciences*, 44, pp. 933-940.

Christensen, G.E., Miller, M.I., Vannie, M., 1994, "A 3-D deformable magnetic resonance textbook based on elasticity," *AAAI Spring Symposium Series: Applications of Computer Vision in Medical Image Processing*, pp. 153-156.

Christensen, G.E., Rabbit, R.D., Miller, M.I., 1996, "Deformable Templates Using Large Deformation Kinematics," *IEEE Transactions on Image Processing*, Vol. 5(10): pp. 1435-1447.

Evans, C., Dai, W., Collins, D.L., Neelin, P., Marret, S., 1991, "Warping of a computerized 3-D atlas to match brain image volumes for quantitative neuroanatomical and functional analysis," *Image Processing, SPIE*, Vol. 1445, pp. 236-246.

Frandsen, M.W., Wessol, D.E., Wheeler, F.J., 2001, "Methods and Computer Executable Instructions for Rapidly Calculating Simulated Particle Transport Through Geometrically Modeled Treatment Volumes Having Uniform Volume Elements for Use in Radiotherapy," U.S. Patent 6,175,761 B1, Issued January 16, 2001.

Frandsen, M.W., Wessol, D.E., Wheeler, F.J., Starkey, D., 1998a, "Rapid Geometry Interrogation for Uniform Volume Element-Based BNCT Monte Carlo Particle Transport Simulation," *Proceedings of the Eighth International Symposium on Neutron Capture Therapy*, La Jolla, CA, USA, Plenum Press, New York.

Frandsen, M.W., 1998b, "*Rapid Geometry Interrogation for a Uniform Volume Element-based Monte Carlo Particle Transport Simulation*," M.S. Thesis, Montana State University.

Ganapol, B.D., et al., 1994, "The Searchlight Problem for Neutrons in a Semi-Infinite Medium," *Nuclear Science and Engineering*, 118, pp. 38-53.

Gee, J. C., Reivich, M., Bajcsy, R., 1993, "Elastically deforming 3D atlas to match anatomical brain images," *Journal of Computer Assisted Tomography*, Vol. 17(2), pp. 225-236, March 1993.

Gosling, J., Joy, B., Steele, G., 1996, *The Java Language Specification*, Addison-Wesley.

Kruger J., Westermann, R., 2003, "Linear algebra operators for the GPU implementation of numerical algorithms," *ACM Transactions on Graphics*, Vol. 22, pp. 908-916, July 2003.

Larsen, E.S., McAllister, D., 2001, "Fast matrix multiplies using graphics hardware," *Proceedings: Supercomputing 2001, ACM SIGARCH/IEEE*, November 2001.

Lefohn, E., Kniss, J.M., Hansen, C.D., Whitaker, R.T., 2003, "Interactive Deformation and Visualization of Level Set Surfaces Using Graphics Hardware," *IEEE Visualization*, pp. 75-82.

Lewis, K., 2000, *Creating Effective JavaHelp*, O'Reilly and Associates.

Rumpf, M., Strzodka, R., 2001, "Using graphics cards for quantized FEM computations," *IASTED Visualization, Imaging and Image Processing Conference*.

Strzodka, R., Rumpf, M., 2001, "Level set segmentation in graphics hardware," *Proceedings ICIP*, pp. 1103-1106.

Ziff, R.M., 1998, "Four-tap Shift-register-sequence random number generator," *Computers in Physics*, 12(4), pp. 385-392.

EPITHERMAL NEUTRON BEAM DEVELOPMENT FOR PRECLINICAL NEUTRON CAPTURE THERAPY RESEARCH AT WASHINGTON STATE UNIVERSITY

J.R. Venhuizen[1], D.W. Nigg[1], J.K. Hartwell[1], C.A. Wemple[1], R.E. Mitchell[1], G.E. Tripard[2], K. Fox[2], D. Duggan[2], J. Fidel[2]

1. Idaho National Laboratory, Idaho Falls, ID
2. Washington State University, Pullman, WA

INTRODUCTION

Veterinary radiation oncology researchers at the Washington State University (WSU) School of Veterinary Medicine, with collaborative technical assistance from the Idaho National Laboratory (INL), have made significant, historical contributions to the understanding of the *in-vivo* biochemistry and radiobiology of Boron Neutron Capture Therapy (BNCT). For example, the large-animal model studies of normal brain tissue tolerance conducted by this group (Gavin et al. 1994, 1996, 1997), provided a key component of the radiobiological basis for the resumption in 1994 of human BNCT trials in the U.S. Those studies used the epithermal-neutron beams available at Brookhaven National Laboratory and at the Petten facility, in The Netherlands, with technical support from the INL in several areas of physics, biophysics, and analytical chemistry. In that work, INL provided experimental neutron dosimetry, computational treatment planning using specialized software developed for the purpose (Nigg 1994; Nigg et al. 1997) as well as precision measurements of boron content in various tissues, blood, and urine of each experimental subject (Bauer et al. 1989, 1992, 1993a, 1993b).

More recently, INL and WSU have collaborated in the construction of a more convenient and cost-effective epithermal-neutron beam facility for BNCT research and borated pharmaceutical screening in large animal models on site at WSU (Wheeler and Nigg 1994; Burns 1996; Nigg et al. 2002; Venhuizen 2001, 2002, 2003). The new neutron beam extraction facility, which will also have a capability to produce a source of thermal neutrons for small-animal research and cell studies, is now in full-power operation at the WSU Nuclear Radiation Center.

This article summarizes the construction and current characterization of the full-power epithermal-neutron beam at WSU. For completeness, previous years' work related to the construction of the beamline components is first summarized, followed by a description of specific accomplishments during 2004, which includes the final wall covering in the treatment room, as well as initial measurements conducted to verify the thermal neutronic performance of the beam with the heavy water (D_2O) moderator installed in the collimator.

FACILITY DESCRIPTION

In the early 1990s, having experienced the considerable logistic difficulties and transportation expenses that were associated with performing large-animal model research using the geographically distant Brookhaven Medical Research Reactor, WSU and INL initiated a feasibility study for construction of a suitable epithermal neutron beam facility using the existing TRIGA[a] research reactor at the WSU Nuclear Radiation Center (Wheeler and Nigg 1994). TRIGA research reactors have long been recognized as suitable neutron sources for BNCT (Whittemore 1992). They have very robust passive safety features and, in the case of the WSU installation, there is excellent direct access to the reactor core, facilitating the construction of the required neutron beam extraction component assembly. Construction of the new epithermal beam facility was completed in 2003 with the installation of online beam monitoring instrumentation and a major reconfiguration of the WSU reactor core to optimize the beam intensity.

The 1 MW WSU reactor core is suspended from a movable bridge above the pool as shown in Figure 1. It can be positioned directly adjacent to a truncated aluminum cone that extends horizontally into the reactor pool from the tank wall on the upstream side of the filtering and moderating assembly. This cone and the adjacent thermal column area were originally filled with graphite, comprising the thermal neutron column (or thermal column) for the WSU Nuclear Radiation Center. A water-filled shield was located on the downstream of the graphite thermal column. Figure 2 shows a schematic diagram of the WSU epithermal-neutron beam facility. The new epithermal-neutron beam extraction components are located in the thermal-column region of the reactor-shielding monolith. The original graphite has been removed from this region and replaced with a new epithermal-neutron filtering, moderating, and collimating assembly as shown. Neutrons emanating from the core travel into the filtering and moderating region. The spectrum is tailored in this region such that most neutrons emerge with energies in the epithermal energy range (0.5 eV – 10 keV). Downstream of the filtering and moderating region is a bismuth and lead gamma shield, followed by a conical neutron collimator composed of bismuth surrounded by borated polyethylene. Provision is made for several different exit port aperture sizes as shown. A heavily shielded concrete beam stop and treatment room has been constructed just outside of the thermal column opening in the reactor shield wall as shown in Figure 3.

A key distinguishing feature of the WSU facility is the incorporation of a high-efficiency, neutron moderating and filtering material Fluental™ developed by the Technical Research Centre of Finland (Auterinen and Hiismäki 1993) into the design. Fluental is manufactured by hot isostatic pressing of a mixture of 69% (by weight) aluminum fluoride, 30% aluminum, and 1% lithium fluoride. A block of this material having a thickness in the beam propagation direction of 0.64 m and transverse dimensions of approximately 0.6 m is surrounded by aluminum oxide to produce the neutron filtering and moderating region shown in Figure 2. MCNP (Breismeister 2000) and DORT (Rhoades 1993) radiation transport design calculations for the coupled core and filter-collimator assembly indicated that a free-beam epithermal neutron flux of approximately

[a] TRIGA is a trademark of General Atomics of San Diego, CA.

10^9 n/cm^2-s at a reactor power of 1 MW would be produced at the irradiation point (with the reactor core optimally loaded). The background neutron KERMA rate per unit useful

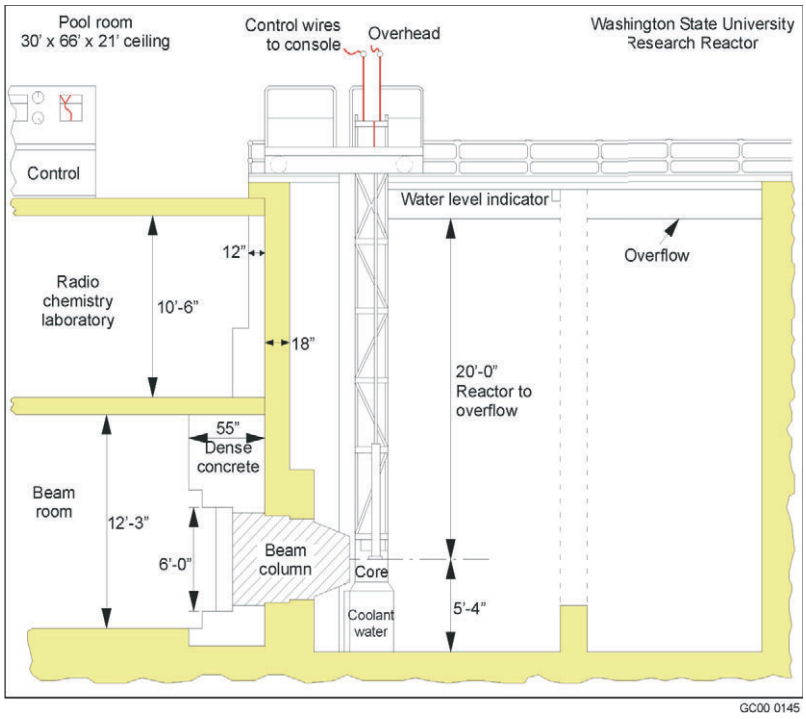

Figure 1. Elevation plan of the WSU TRIGA reactor facility.

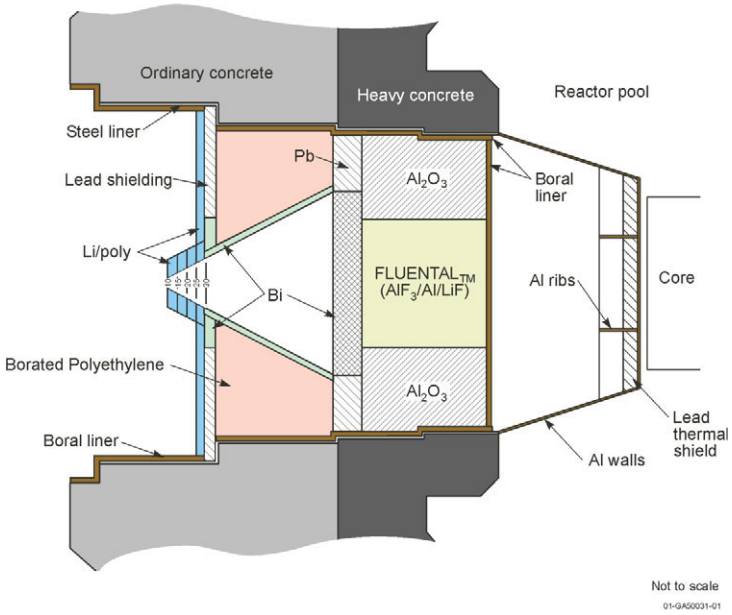

Figure 2. WSU column assembly, with epithermal neutron filter in place.

epithermal neutron flux (a measure of the fast-neutron contamination) for the beam was calculated to be approximately 3.0 x 10^{-11} cGy/n-cm^2. The computational methods used for this design were previously validated against INL measurements performed for a similar neutron beam facility that is already in operation at the FiR 1 TRIGA research reactor in Finland (Nigg et al. 1999, 2001).

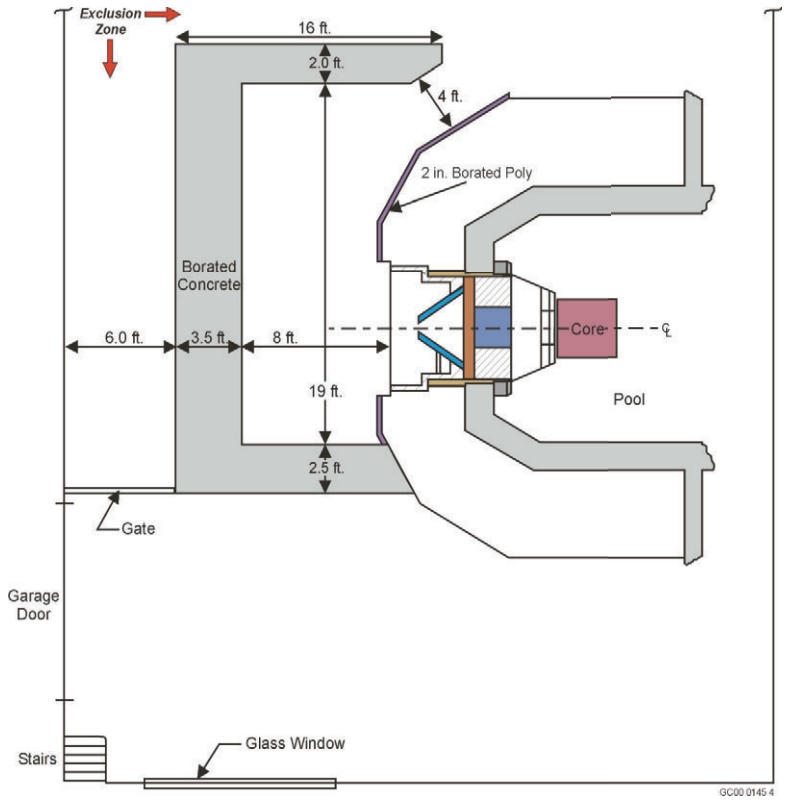

Figure 3. Approximate WSU beam stop and treatment room arrangement (top view).

An additional key feature of the WSU beam facility design is the provision for adjustable neutron spectra. The filter-moderator thickness can be changed to systematically explore the radiobiological consequences of increasing the fast-neutron contamination above the nominal value associated with the baseline system described above. This is an important clinical issue for BNCT (Alpen et al. 1993). Thinner filter/moderator arrangements will produce epithermal beams having correspondingly harder spectra and greater levels of fast-neutron contamination. The beamline components shown in Figure 2 are designed for relative ease of disassembly and re-assembly compared to other reactor-based epithermal-neutron facilities that are currently in operation. Thus, it would be possible to have a number of different filter/moderator arrangements over the life of the facility. It should also be noted that provision has been made to fill the collimator region with heavy water (D_2O) to provide an option for a thermalized neutron beam for cell and small animal studies. This is achieved via a triple-walled plastic liner inside of the collimator, coupled with a bismuth end cap placed over the collimator exit. Testing of the beam thermalization components was completed in the latter half of 2004.

SUMMARY OF BEAMLINE CONSTRUCTION AND INSTRUMENTATION

Construction of the new WSU beam facility began by removing the existing graphite from the thermal column. In other facility work, sponsored by the State of Washington, the reactor tank was drained and completely refurbished, and the main heat exchanger was replaced. In the meantime, the Fluental beamline filter/moderator components were machined by VTT Finland to INL specifications and delivered to WSU. These components were first assembled on the reactor floor to verify the dimensions. In addition, the necessary aluminum oxide beamline components were fabricated by Coors Ceramics and delivered to WSU.

Beamline Component Installation

Prior to installation of the filter-moderator components, it was deemed necessary to place thermocouples at selected locations on the primary gamma shielding at the upstream end of the thermal column cone housing, as shown in Figure 4. This shielding is composed of lead and is (by design) subject to heavy gamma heating from the adjacent reactor core. Hence, the temperature must be monitored to verify a suitable temperature margin.

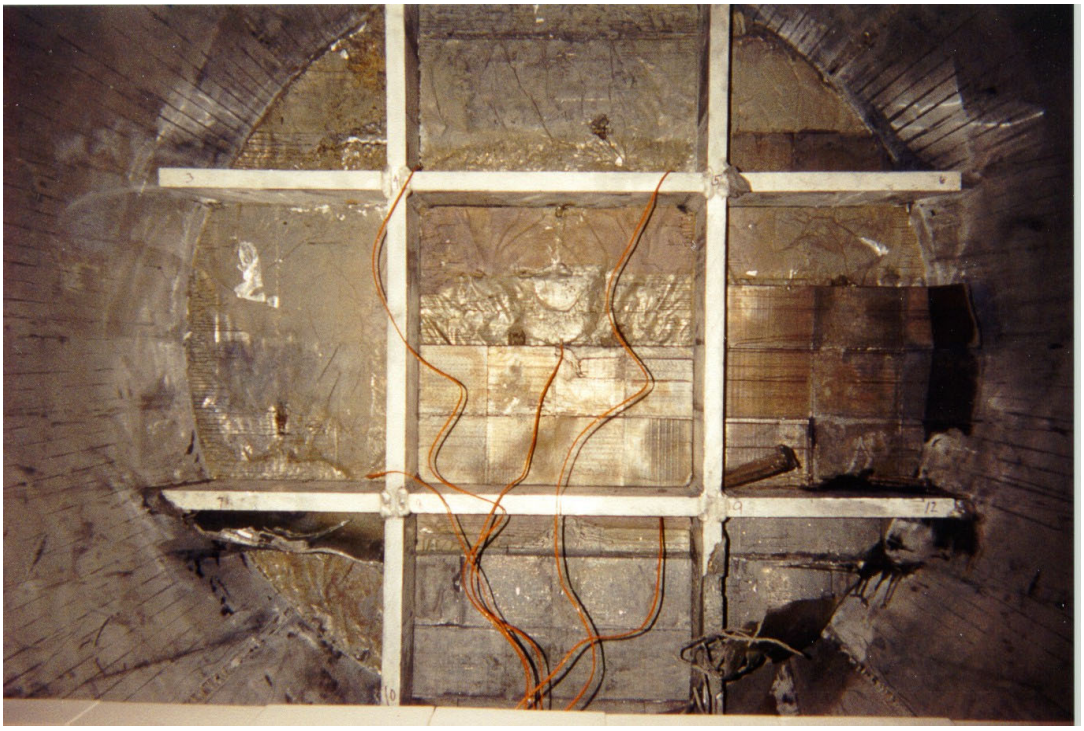

Figure 4. Thermocouple installation in the upstream gamma shielding region of the WSU thermal column cone.

The primary filter moderator-filter assembly was then built up from blocks of aluminum oxide and Fluental as shown in Figure 5 for the partially completed assembly and for the fully completed assembly.

Figure 5. Partially completed (left) and fully installed (right) WSU filter-moderator assembly.

Following the installation of the filter-moderator assembly, the concrete walls and ceiling of the treatment room were constructed. The partially completed treatment room, prior to pouring of the roof, is shown in Figure 6. During the two-month period of time required for this part of the project, bismuth blocks for the final gamma shield were fabricated.

Figure 6. WSU treatment room walls during construction.

Four interlocking bismuth gamma shield blocks were cast at the INL. When the treatment room was completed and access to the thermal column was again possible, these blocks were installed as shown in Figure 7. The bismuth bocks, which span the central part of the filter-moderator, are surrounded by standard lead shielding blocks. Prior to installing the shield blocks, the entire filter-moderator assembly was covered by 1-mm (40-mil) of cadmium using 30.5 cm (12 in.) vertical strips (also shown in Figure 7) in order to suppress thermal neutrons in the final beam.

Figure 7. Cadmium thermal neutron shield and bismuth-lead gamma shield during installation at WSU.

Figure 8 shows the collimator installation. The collimator, comprised of 16 identical bismuth "barrel-stave" castings to facilitate assembly and disassembly without heavy lifting equipment, is a truncated right circular cone with a base opening diameter of 91.4 cm (36 inches), a height of 38.1 cm (15 inches), and a wall thickness of 3 cm (1.2 inches). The angle of the cone is 45 degrees. It is supported by borated polyethylene and two rows of lead bricks as shown in Figure 8b. The downstream end of the collimator is fitted with a bismuth collar designed to provide a transition from circular shape of the cone to the square shape required to match with the lead shielding bricks comprising the final shield wall. The collar will accommodate borated or lithiated polyethylene inserts having various beam port aperture sizes and field shaping configurations. The staves and collar were also cast at INL using specialized techniques designed for the purpose. Finally, Figure 9 shows the positioning of the final lithiated polyethylene neutron suppression shield on the outer surface of the bismuth-lead shield wall as well as the beam exit port with a 10-cm aperture shaping plate in place.

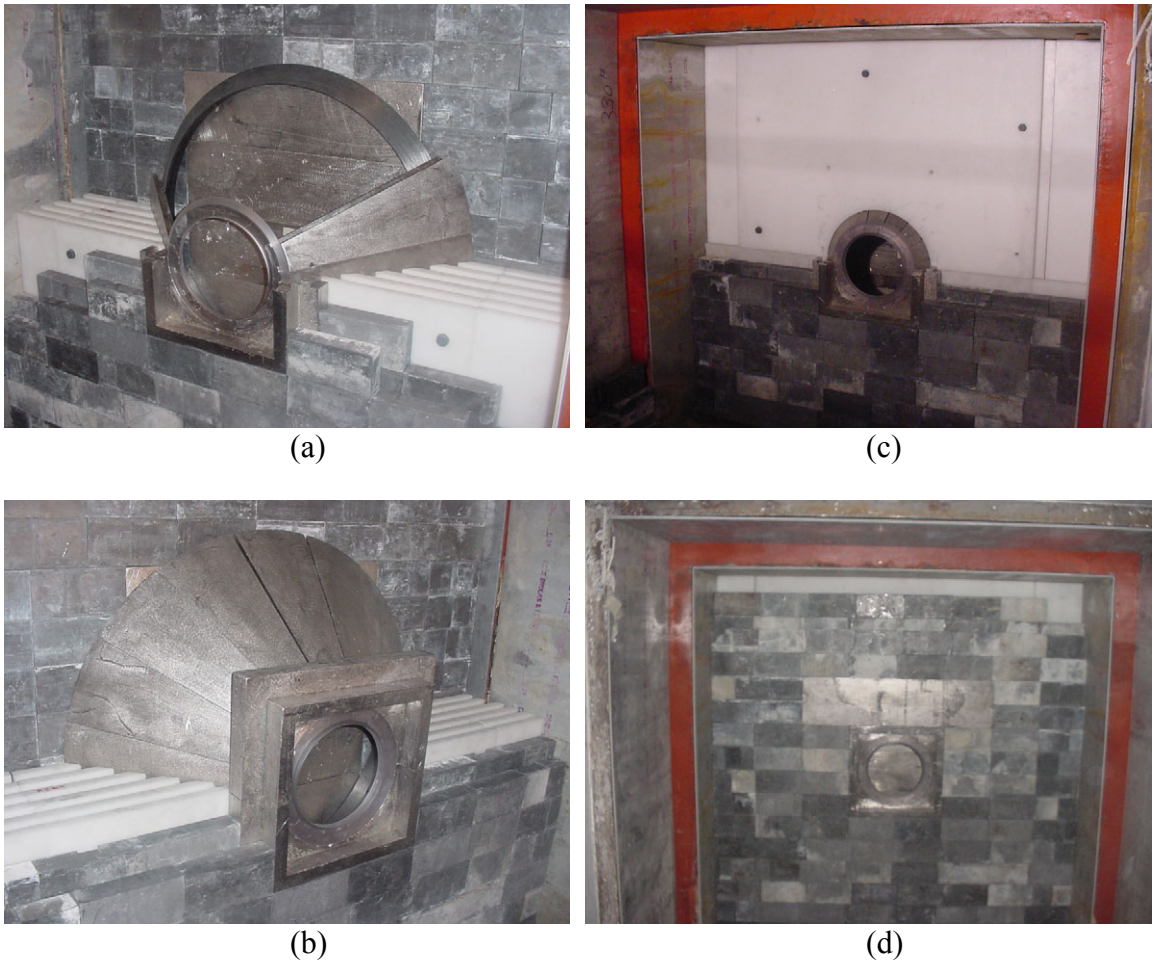

(a) (c)

(b) (d)

Figure 8. Final beam collimator installation at WSU showing the partially installed collimator (a), the fully installed collimator with square exit port collar and lower borated polyethylene shielding (b), the upper borated polyethylene shielding (c), and the final lead shielding (d).

Figure 9. Lithiated polyethylene neutron suppression shield and beam aperture plate arrangement for the 10-cm diameter beam exit aperture at WSU.

In early 2004, the ceiling and sidewalls were covered with 1 inch thick natural lithiated polyethylene (7.5% Lithium-Polyethylene, Thermo-electron Cat. No. 215) to reduce the reflected neutrons without generating additional gamma radiation. Two fluorescent lights were added in the upper corners. Figure 10 shows the completed structure. To reduce activation, no metal fasteners were used in the construction.

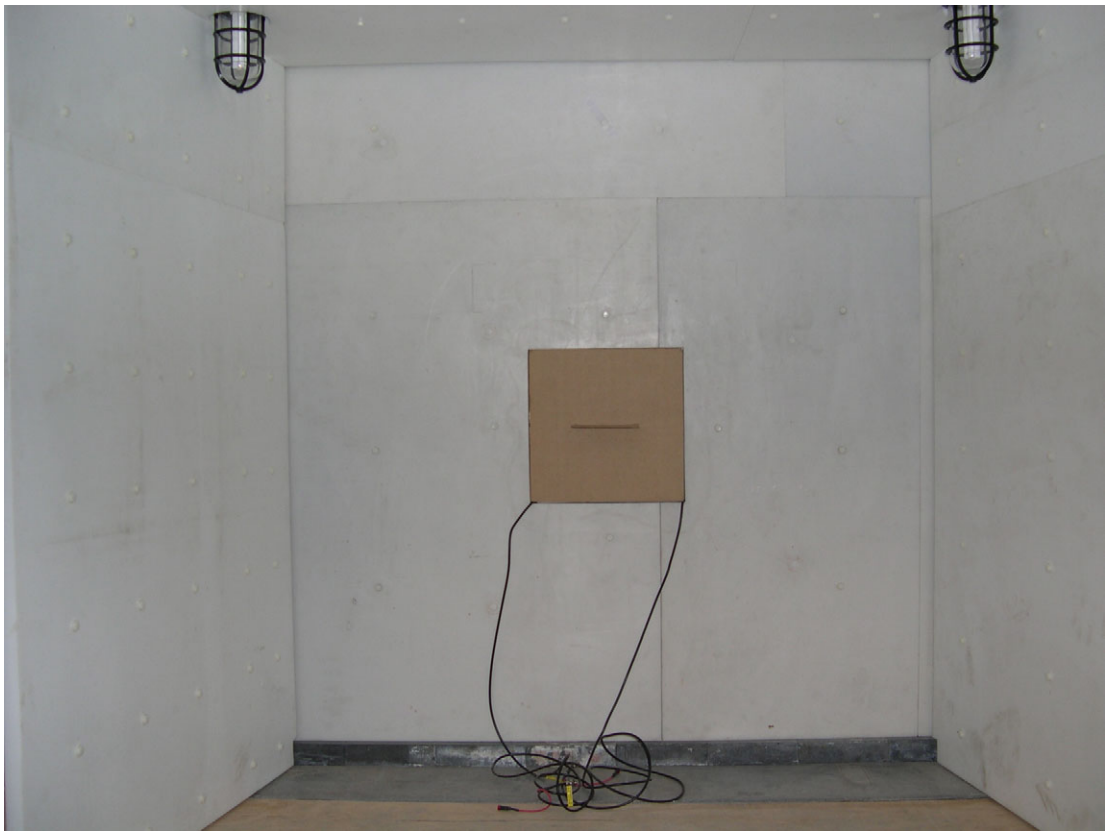

Figure 10. Lithiated polyethylene lined walls and ceiling of beam room. Lights are shown in the corners. Fission chamber cables are also visible in the photo.

The neutron thermalization beamline component was installed and tested in 2004. Since there are requirements for thermal neutrons for small animal (mice-rats) studies, an investigation was made to determine a suitable means to thermalize the WSU beam. The result of the investigation indicated that heavy water (D_2O) was the best moderator while allowing maximum neutron flux at the exit. A polyethylene double-walled bag system was designed by INL researchers to fit inside the collimator. This double bag was then inserted in a single wall bag, giving a triple containment system (bags mfg. by Interstate Plastics, Boise ID). Figure 11 shows the bags inflated with nitrogen prior to installation in the collimator volume. The 'top' is the right hand side of the figure. The fill/drain and vent hoses (Tygon tubing) are shown coming out the top of the single wall bag.

Figure 11. Polyethylene bags inflated with nitrogen.

Figure 12 shows the bags installed in the collimator with the hoses and the fission chamber cables protruding from the opening. Figure 13 shows the hoses and cables threaded through the bismuth retainer plate. This plate restrains the water filled bags in the collimator. The bismuth plate is bolted to the collimator collar.

Figure 12. Polyethylene bags installed in the collimator. Tygon fill and vent lines are shown.

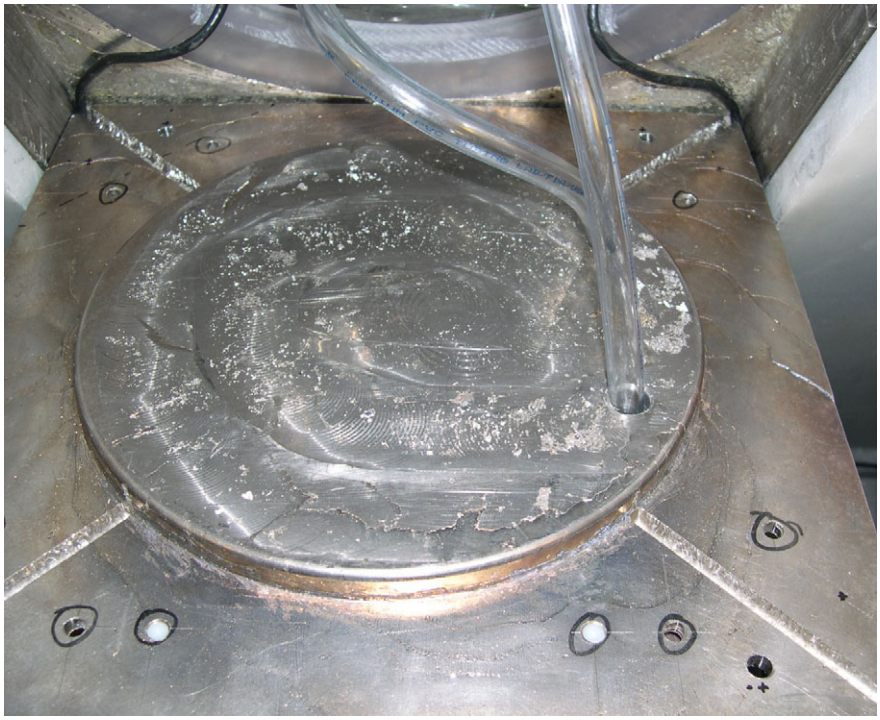

Figure 13. Bismuth retainer plate with fill/drain hoses inserted.

Figure 14. Bismuth plate installed in collimator opening. Four corner bolts are threaded into the bismuth collar. Cables are connected to the fission chambers.

The heavy water was pumped into the bag from two 15-gallon containers. Prior to filling the bag, the liquid level in the containers was noted so that all the heavy water could be accounted for when removed from the bag. Since the heavy water becomes tritiated with neutron exposure, the heavy water was treated as contaminated when it was drained from the bag. The tritium buildup was calculated to be approximately 1.1×10^{-3} microcuries per milliliter per hour of full power (1 MW) operation. The measured tritium concentration after one-hour full power operation was 0.93×10^{-3} microcuries per milliliter.

On-Line Instrumentation

Because the WSU facility is, at least for the foreseeable future, intended only for animal studies, it has been possible to achieve some economies by simplification of the online instrumentation compared to what is required for BNCT facilities used for human trials. The primary beam monitor is based on redundant fission chambers (GE Reuter-Stokes Model RS-P6-0402-101) mounted on the inside of the collimator, approximately halfway between the bismuth shield face and the collimator exit. These chambers were installed and tested in late FY 2003.

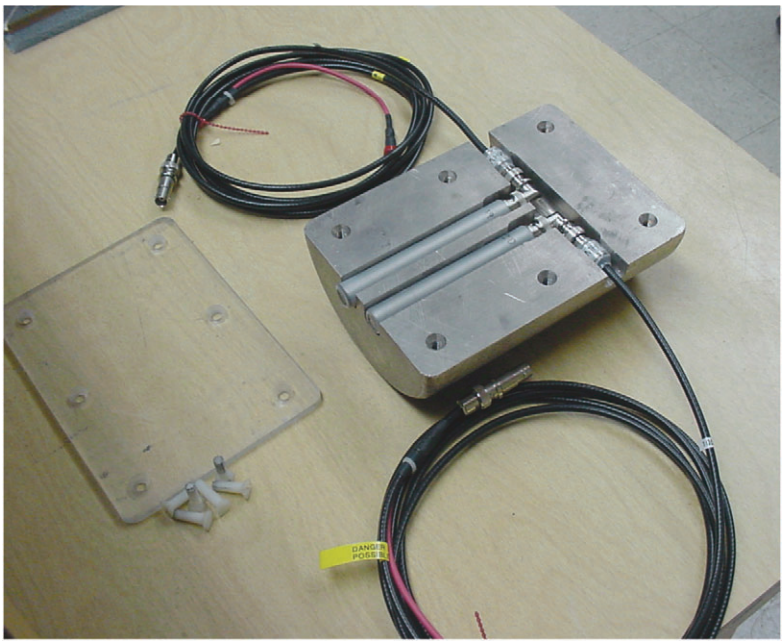

Figure 15. Fission chambers positioned in bismuth shield prior to insertion into the bismuth collimator. Note the insulation (shrink tubing) on the chambers and MHV connectors. The Lucite plate keeps the chambers in place.

Figure 15 shows the fission chamber assembly prior to insertion into the collimator. The cadmium-covered fission chambers were surrounded on the upper side with 5 cm of bismuth for a gamma shield. Since the chambers are made of aluminum and the electrical connectors are made of steel, these items, along with the cadmium covers, will become activated when exposed to neutrons. The bismuth shield was thus provided in

order to reduce the gamma exposure at the collimator exit due to this activation as well as from the fission products formed in the chambers themselves. These fission chambers, operated in current mode, form the basis for an independent online epithermal neutron monitor not tied to the reactor power measurement.

The electrometers used with the fission chambers are Unidose E made by PTW-Frieburg. The fission chambers are operated at 250 volts. They can be used to measure current or can integrate charge for set time periods. There is a provision for continuous monitoring and data storage by computer via a serial port.

Figure 16 shows the upper side of the fission chamber shield, prior to installation and after installation on the lower inside surface of the collimator. It was confirmed by measurement with and without a large Lucite phantom at the exit port that the response of the fission chambers in this location is insensitive (<2% variation) to the presence or absence of hydrogenous scattering material at the exit port.

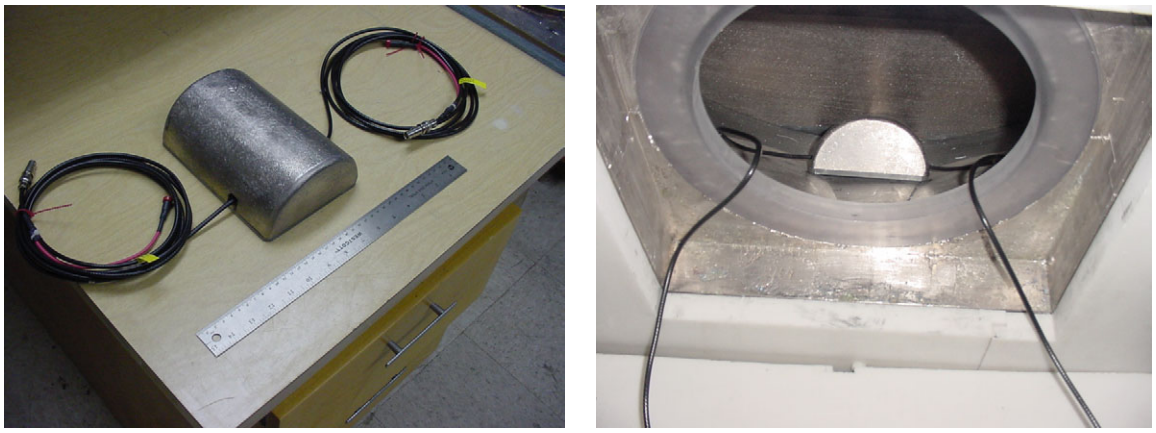

Figure 16. Fission chamber gamma shield prior to (left) and after (right) insertion into the bismuth collimator.

The incident gamma field in the beam is currently measured using a Radcal Corporation Model 9010S with a model 10X5-0.6 ion chamber. The ion chamber, which has a 0.6 cm^3 active volume and 1 μGy/min to 74 Gy/min rate sensitivity, is positioned at the exit plane of the beam when measuring the free-beam gamma dose rate.

Figure 17. WSU treatment room showing the ambient neutron monitor (Bonner sphere) in the upper right corner. The neutron beam exit port is to the left in the figure.

The ambient neutron and gamma fields in the treatment room are measured using a combined neutron-gamma instrument (Ludlum Model 375) composed of a Bonner sphere surrounding a BF_3 chamber, and a separate Gieger-Muller gamma monitor mounted nearby. Figure 17 shows the location of these instruments in the treatment room. The epithermal neutron beam port is just inside the thermal column cavity on the left side of the figure.

Standard Dosimetry Phantom

A Scandtronix clinical water phantom with a 3-dimensional positioning system (Therados Model RFA-3) was positioned in the beam as shown in Figure 18. This system was originally developed for calibration of photon therapy machines, and modified for use with the neutron facility. Only the 3-axis drive and positioning system, water tank, and position readout are being utilized for neutron measurements. The tank was filled with de-ionized water. A paired set of tissue-equivalent and graphite ion chambers (Far West models 784 TTW and 773-TGW, respectively) was installed in the water phantom, and initial testing of the overall system with the unoptimized neutron beam was completed in 2003. The Unidose-E electrometers were used for the readout. Specifications for this system are consistent with the recommendations of the International NCT Dosimetry Exchange (Järvinen and Voorbrack 2003) for a reference dosimetry phantom of this type.

Figure 18. Water phantom at WSU (left), with detail of paired ion chamber arrangement (right).

Reactor Core Fuel Reconfiguration

In the final step of the beam installation, the WSU reactor fuel-loading configuration was modified in late calendar year 2003 to substantially shift the spatial peak of the fission distribution toward the side of the core immediately adjacent to the epithermal beamline entrance. Calculations indicated that this would roughly triple the beam intensity.

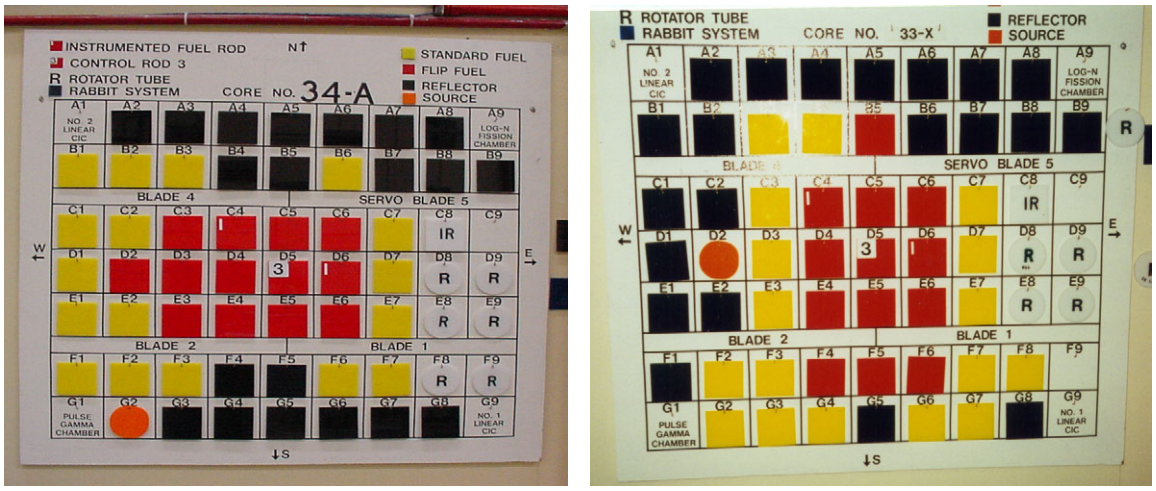

Figure 19. New core loading pattern (left), compared with previous fuel loading pattern (right). Yellow squares are standard low-enriched fuel, red squares are high-enriched fuel, and black squares are graphite reflectors. The epithermal beamline entrance is adjacent to the left side of both diagrams.

Figure 19 shows the new fuel-loading pattern compared with the previous loading. Specifications for the new loading pattern were developed by the INL using an MCNP computational model of the reactor. Independent calculations were performed by WSU to confirm the results. In general, the desired flux shift was achieved by removing

graphite reflector elements on the side of the core adjacent to the beamline entrance, replacing these with low-enriched fuel, and shifting the highly-enriched section of the core toward the same side. In addition, the startup source was moved to a new position, away from the beamline entrance as shown, and replaced with highly enriched fuel.

PERFORMANCE VALIDATION FOR THE OPTIMIZED BEAM

Measurements of the free beam spectrum and some in-phantom beam performance measurements were conducted by INL and WSU at several points during the final construction phases to establish that the beam performance was within the expected range. These measurements included simplified neutron foil activation measurements for the free beam, a few basic phantom measurements using foils and flux wires and, finally, a free beam measurement based on counting of radiation-induced nucleation sites in specialized superheated materials (Apfel et al. 1979, Nath et al. 1993) to provide improved detail in the above-epithermal energy range. These early measurements are well documented elsewhere (Venhuizen et al. 2001, 2002, 2003) and the details will not be repeated here. In addition, a visiting representative of the European team of the International NCT Dosimetry Exchange (Harling et al. 2002) performed some preliminary independent measurements of the beam in early 2003, prior to the reconfiguration of the core.

The discussion here will focus only on a summary of the basic free beam measurements conducted by INL and WSU in late 2003 to confirm the intensity and spectrum of the final beam after the core fuel reconfiguration was completed. More detailed characterization measurements are planned for 2005. It is anticipated that these measurements may also include continued participation of WSU in the International NCT Dosimetry Exchange (Järvinen and Voorbrack 2003).

The free beam neutron spectrum measurements reported here are for an imaginary transverse "source plane" passing through the base of the square flange on the downstream side of the bismuth collimator collar (see Figure 8b). The source plane is a mathematical construct used for specifying the neutron source boundary conditions for the various dosimetry and treatment planning computations required to support each experimental irradiation. By definition, the physical beamline components upstream of the source plane do not change from one irradiation to the next. Components downstream of this plane, such as the field shaping plates, can change for each irradiation and, therefore, are explicitly modeled in dosimetry and treatment planning computations. Time-consuming beam modeling computations are thus done only once for each beamline configuration upstream of the source plane, and the results are coupled to the patient dosimetry computations for each irradiation via a computed boundary condition specified for the source plane and validated by appropriate measurements.

The measurements were based on a simplified version of an activation foil protocol that has been adapted for BNCT applications by the INL through extensive experience with several other epithermal-neutron and fast-neutron facilities worldwide (Harker et al. 1992; Nigg et al. 2000). Standard 12.7-mm diameter cadmium-covered In, Au, W, Mn,

Co, Cu, and Sc foils were used with a positioning plate made of Lexan™ as shown in Figure 20. An uncovered gold foil was also placed in an outer position of the foil plate. The foils had nominal thicknesses in the range of 0.0254 mm to 0.127 mm, depending on the material type.

Figure 20. Source plane activation foil plate (left) positioned in the WSU epithermal neutron beam source plane (right). The boron sphere is shown in the center of the plate assembly.

Figures 21 and 22 show an additional aluminum foil wheel that also has been used in spectrum measurements. This wheel is inserted into the 10 cm exit port of the lithium or borated polyethylene collimators.

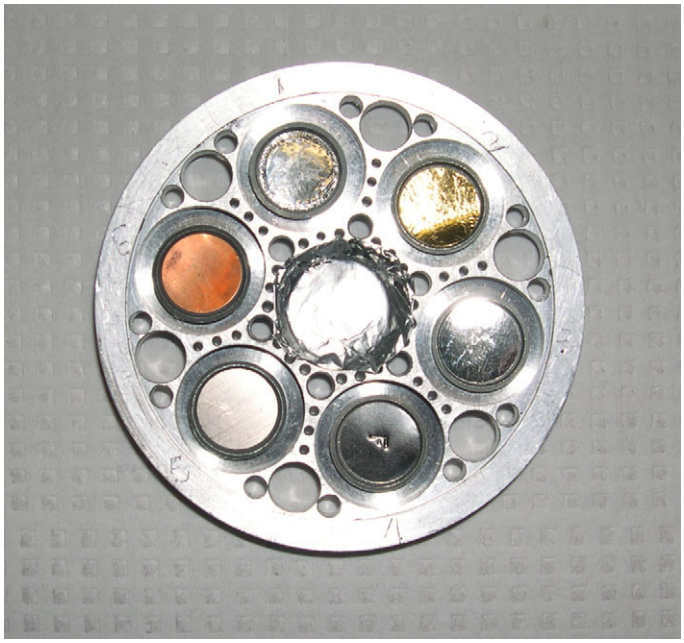

Figure 21. Close-up of the foil wheel without the Cd covers in place.

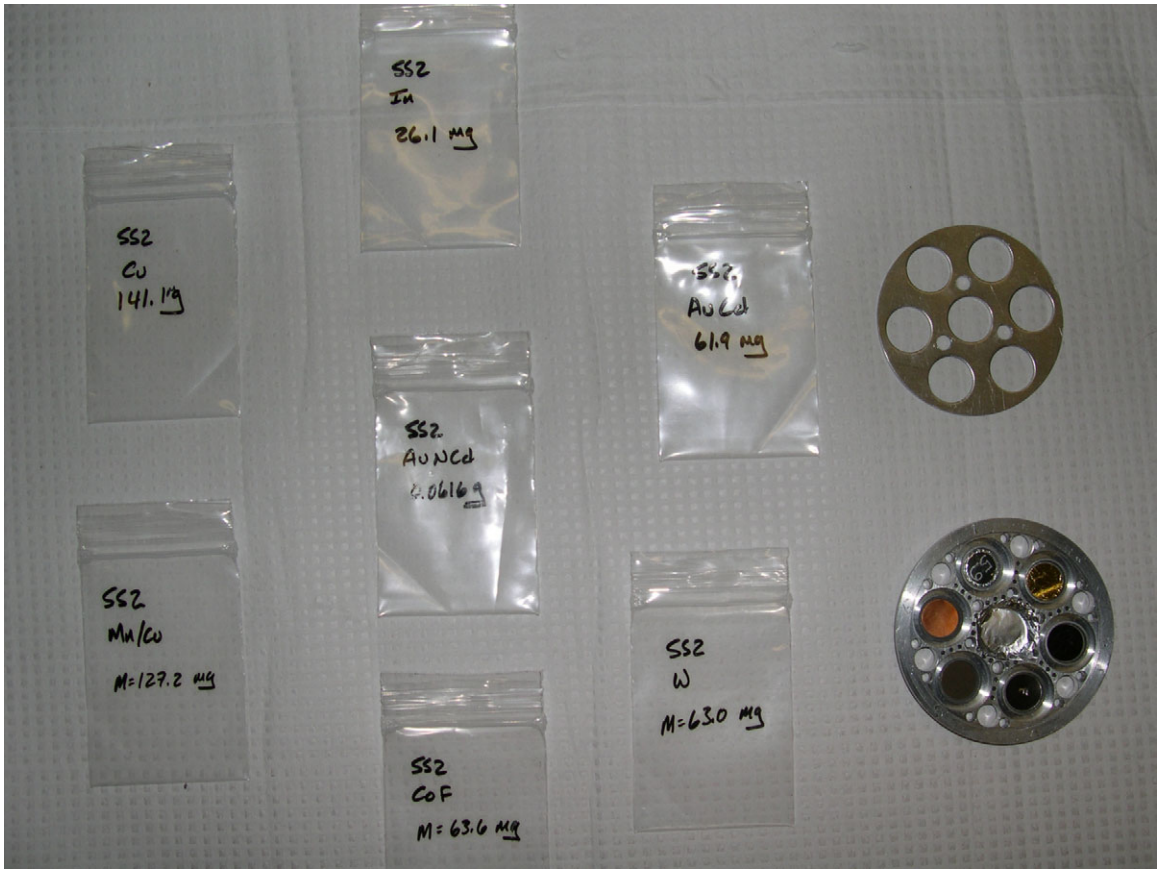

Figure 22. Foil wheel assembly layout.

An additional foil was used to provide key spectral information in the energy range above epithermal (E >10 keV). A heavy (~5 g) 25.4-mm diameter indium foil was placed in a small hollow boron sphere (inside diameter 2.8 cm, outside diameter 4.75 cm) located in the center of the foil positioning plate. The composition of the sphere, shown in Figure 23, is approximately 93% ^{10}B and 7% ^{11}B by weight, with a total boron density of 2.6 g/cm^3. This arrangement provides essentially total suppression of thermal and epithermal neutrons within the inner cavity of the boron sphere. Thus, an artificial threshold above the resonance neutron capture energy range for indium is imposed on the foil within the sphere. Since the activation gamma emissions that arise from neutron capture in indium are thereby suppressed, the relatively weak 336 keV gamma line from inelastic scatter in indium, which is of crucial interest in these measurements, is much more prominent in the spectrum of the activated indium foil.

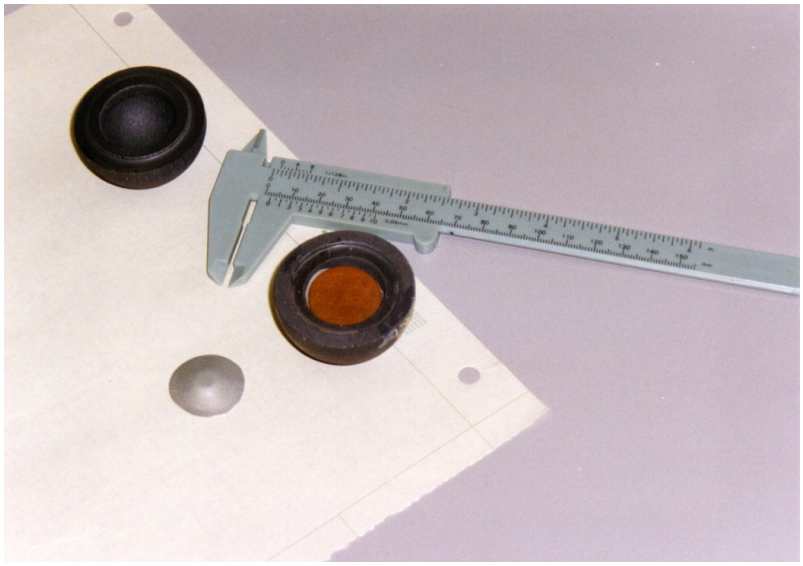

Figure 23. Boron sphere used to suppress low-energy neutron flux.

The irradiated foils were assayed at WSU using a standard high-purity germanium (HPGe) gamma spectrometry system (Canberra/Genie^{TM}). The induced activities in the free-beam foils were computed from the photopeak areas and system efficiencies based on calibration of the spectrometer using a National Institute Standards and Technology (NIST)-traceable mixed europium-antimony calibration source. The measured activity of the heavy indium foil in the boron sphere was corrected for gamma self-shielding using an escape fraction at 336 keV calculated using a combination of MCNP computations and handbook data for the specific source-detector geometry that was used for the assay. This factor was 0.90±0.01. The measured activation rates of the various foils were then used to estimate the neutron spectrum by way of an over determined least-squares matrix unfolding procedure (Nigg et al. 2000).

Figure 24 shows an unfolded 6-group free-field unperturbed neutron spectrum in the source plane, projected by the unfolding process to the center of the foil positioning plate. The computed 47-group *a-priori* neutron spectrum, normalized to 1 MW, is also shown for comparison. The broad group structure used for calculation of the unfolded spectrum from the data for the eight activation interactions considered was selected to provide a well-conditioned unfolding matrix, and to permit an accurate integration of the measured spectrum in the epithermal energy range to determine the total epithermal neutron flux.

Integrating the measured curve over the epithermal energy range (0.5 eV – 10 keV) produces a total epithermal neutron flux of 1.66 x 10^9 n/cm^2-sec at 1 MW with a propagated uncertainty of approximately 5% (1σ). An alternate estimate of the measured spectrum from the activation data using a method based on the SAND-2 code (McElroy et al. 1967) as described by Draper (1971) yielded a very similar result for the epithermal flux: 1.54 x 10^9 n/cm^2-sec. In both cases this is almost exactly three times the flux produced with the original reactor fuel loading, as expected. This relative intensity

increase was independently confirmed by on-line fission chamber measurements performed using the cadmium-covered GE-Reuter-Stokes fission chambers described previously. Experience with the earlier un-optimized beam showed that the free-beam flux intensity at the irradiation point is reduced by about 20% relative to the source plane flux when using the standard 10.16 cm aperture plate. Thus, the useful flux with that aperture would be approximately 1.3 x 10^9 n/cm^2-sec, well within the accepted range for a useful epithermal beam in terms of intensity (Harling and Riley, 2003).

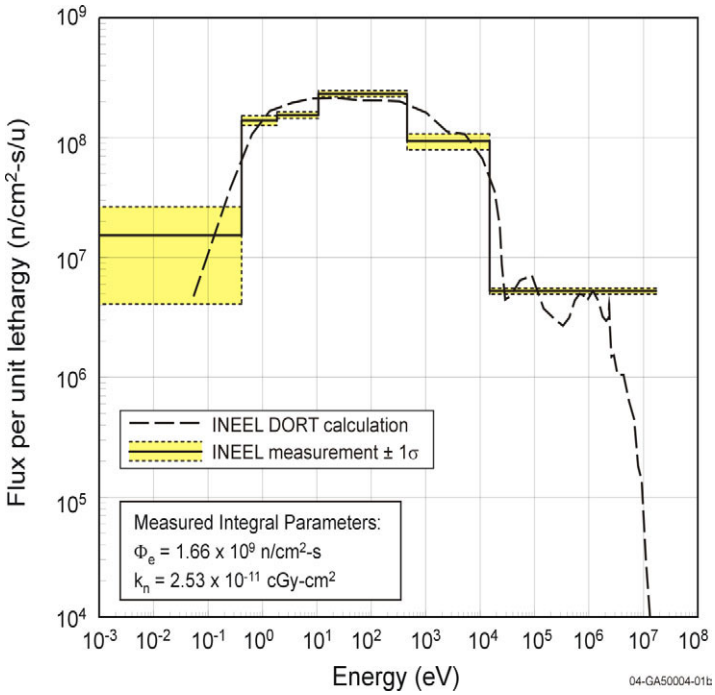

Figure 24. Unfolded free beam neutron spectrum in the source plane obtained by direct fitting for the WSU epithermal neutron beam facility. The reactor power was 1 MW.

It will be observed that the propagated uncertainty associated with the thermal flux (E<0.404 eV) in Figure 24 is quite large. This is a result of the fact that the thermal flux is very small compared to the remainder of the spectrum. The measured activities of the gold foils with and without Cd covers differ by only a few percent. This leads to a magnification of the uncertainty in the usual manner when the thermal flux is estimated from these foil activities in the spectral unfolding process.

A simple, but widely used metric for the biophysical quality of reactor-based epithermal-neutron beams is based on dividing the free-field neutron KERMA rate of the beam (integrated over all energies above thermal) by the useful epithermal-neutron flux, again measured in the free field. This parameter is an indicator of the non-selective neutron background dose that will be produced in tissue by the above-thermal spectral component of the beam itself, in the absence of any neutron capture agent that may be administered to the patient. It is computed here for WSU using the measured flux spectrum in conjunction with broad group KERMA factors based on data for the components of standard tissue available on File 27 of the BUGLE (Roussin, 1980) cross section library.

Fine-group neutron KERMA factors are averaged over the broad unfolding group structure using the *a-priori* spectrum as a weighting function to produce the necessary information. This procedure yields a measured free-beam spectral-average of 2.53×10^{-11} cGy total neutron KERMA from all components per unit useful epithermal-neutron flux, with an estimated uncertainty of about 10%. This is consistent with international beam design guidelines, and is in excellent agreement with the computed value of 2.75×10^{-11} cGy-cm^2. Approximately 91% of the background neutron dose results from proton recoil. The remainder is from other recoil components. Additional background dose in tissue is, of course, produced by non-selective thermal-neutron induced components, primarily from neutron capture in nitrogen and hydrogen, but these components are not directly indicative of the intrinsic biophysical quality of the incident beam. They must be taken into account in treatment planning, but they are not normally included in the free-beam quality parameter discussed here.

FUTURE PLANS

As noted previously, several measurements of the neutron beam performance were conducted at various points during the beamline component installation process. These were basically engineering checks to validate the beam design and to ensure that the performance was within specification at each point during installation. For example, a measurement of this type illustrated the need to install an aluminum plate between the reactor core and the cone entrance, as shown in Figure 25, in order to exclude water from this region. The gap between the core and the face of the cone was greater than expected from the design drawings, and the water in this region severely degraded the beam performance until the plate was installed.

Thus, the types of measurements that have been done so far were for different purposes, and were less comprehensive than the benchmark characterization measurements that are needed now that the beam installation is complete. In FY 2005, a more complete set of characterization and calibration measurements will be documented, following the guidance of the applicable emerging international standard (Järvinen and Voorbrack 2003). Free beam spectrum measurements using multiple foil techniques, with alternate methods of spectral unfolding, will be completed for the final beam at the standard epithermal irradiation location (10 cm aperture, 6.25 cm downstream from the source plane). Measurements conducted for the thermalized beam will also be completed and documented. In addition, flux-mapping measurements using activation wires in various phantoms shown Figures 26 and 27 will be conducted.

Figure 25. View from above into the WSU reactor tank showing the reactor core on the left (in the withdrawn position) and the beam entrance cone on the right, with the aluminum plate in position to exclude water from the region between the core and the cone face when the reactor is in the position for BNCT irradiations.

Figure 26. Lucite cylindrical and canine phantoms (left) and human phantom (right) used at WSU. The photo on the left also shows the upstream side of two-beam aperture shaping plates.

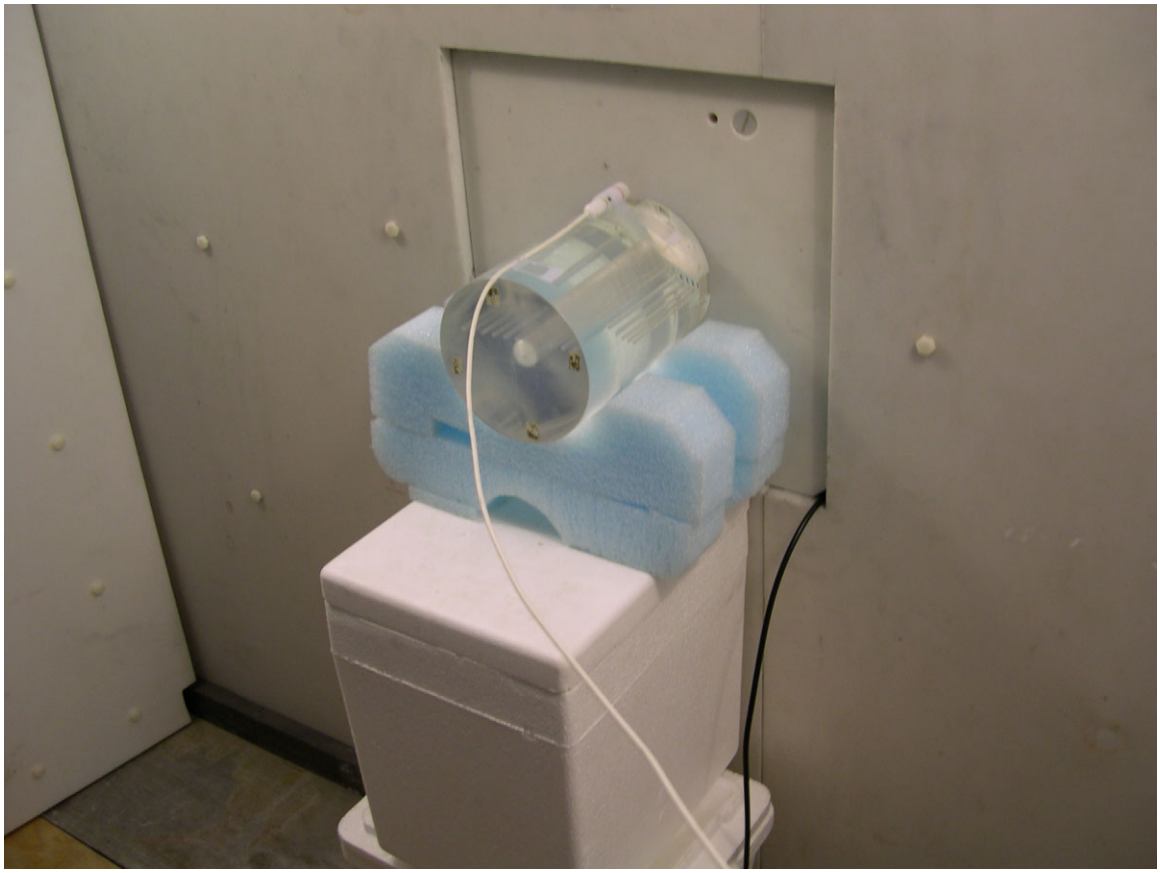

Figure 27. Lucite cylinder in position for axial flux measurement. Radcal gamma probe is taped to top of cylinder.

REFERENCES

Alpen, E.L. and Frankel, K.A., 1993, "Biological effectiveness of recoil protons from neutrons of energy 5 keV to 5 MeV," In: Soloway, A.H., Barth, R.F., Carpenter, D.E. (Editors), *Advances in Neutron Capture Therapy*, Plenum Press, New York, pp 201-206.

Apfel, R.E. and Lo, Y.C., 1979, "Practical neutron dosimetry with superheated drops," *Health Physics* 56:79-83.

Auterinen, I. and Hiismäki, P., 1993, "Epithermal BNCT Neutron Beam Design for a TRIGA II Reactor," In: Soloway, A.H., Barth, R.F., Carpenter, D.E. (Editors), *Advances in Neutron Capture Therapy*, Plenum Press, New York, pp 81-84.

Barth, R.F., Yang, W., Coderre, J., 2003, "Rat Brain Tumor Models to Assess the Efficacy of Boron Neutron Capture Therapy: A Critical Evaluation," *Journal of Neuro-Oncology*, 62:61-74.

Bauer, W.F., Johnson, D.A., Steele, S.M., Messick, K., Miller, D.L., Propp, W.A., 1989, "Gross Boron Determination in Biological Samples by Inductively Coupled Plasma-Atomic Emission-Spectroscopy," *Strahlentherapie Und Onkologie*, 165:176-179.

Bauer, W.F., Wishard, J.A., Rae, C., Lassahn, N., 1992, "Flow injection for sample introduction into inductively coupled plasma for the determination of boron in biological samples," In: Allen, B. J., Moore, D. E., Harrington, B. V. (Editors), *Progress in Neutron Capture Therapy for Cancer*, pp 297-300. New York: Plenum Press.

Bauer, W.F., 1993a, "Analysis of Boron in Biological Samples," *INEEL BNCT Research Program Annual Report-1992*, EGG-BNCT-2700, Idaho National Engineering Laboratory, USA.

Bauer, W., Micca, P, White, B., 1993b, "A Rapid Method for the Direct Analysis of Boron in Whole Blood by Atomic Emission Spectroscopy," In: Soloway A.H., Barth R.F., Carpenter D.E. (Editors), *Advances in Neutron Capture Therapy*, Plenum Press, New York pp 403-408.

Breismeister, J.F., 2000, *MCNP – A General Monte Carlo N-Particle Transport Code, Version 4C*, LA-13709-M, Los Alamos National Laboratory, USA.

Burns, T.D. Jr., 1996, *A Monte Carlo Model System for Core Analysis and Design at the Washington State University Radiation Center*, INEL-95/0458, Idaho National Engineering Laboratory, USA.

Draper Jr., E.L., 1971, "Integral Reaction Rate Determinations - Part I: Tailored Reactor Spectrum Preparation and Measurement," *Nuclear Science and Engineering*, 48:22-30.

Gavin, P.R., Kraft, S.L., DeHann, C.E., Swartz, C.D., Griebenow, M.L., 1994, "Large Animal Normal Tissue Tolerance with Boron Neutron Capture," *Int. J. Radiat. Oncol. Bio. Phys.*, 28:1099-1106.

Gavin, P.R., Kraft, S.L., Swartz, C.D., Wheeler, F.J., Bauer, W.M., 1996, "Boron Neutron Capture Therapy of Spontaneous Intracranial Tumors in Dogs," In: Mishima, Y., *Cancer Neutron Capture Therapy*, Plenum Press, New York.

Gavin, P.R, Kraft, S.L., Huiskamp, R., Coderre, J., 1997, "A Review: CNS Effects and Normal Tissue Tolerance in Dogs," *Journal of Neuro-Oncology*, 33:71-80.

Harker, Y.D., Anderl, R.A., Becker, G.K., Miller, L.G., 1992, "Spectral Characterization of the Epithermal Neutron Beam at the Brookhaven Medical Research Reactor," *Nuclear Science and Engineering*, 110:355-368.

Harling, O.K. et al., 2002, "International Dosimetry Exchange – A Status Report," In: Sauerwein, W., Moss, R., and Wittig, A., *Research and Development in Neutron Capture Therapy*, Monduzzi Editore, S.p.A., Bologna, Italy.

Harling, O.K. and Riley, K.J., 2003, "Fission Reactor Neutron Sources for Neutron Capture Therapy – A Critical Review," *Journal of Neuro-Oncology*, 62:7-17.

Järvinen, H. and Voorbrack, W.P., 2003, "Draft European Commission Standard, Recommendations for the Dosimetry of Boron Neutron Capture Therapy (BNCT)," *NRG,* Petten, The Netherlands.

McElroy, W.N., et al., 1967, "SAND-II Neutron Flux Spectra Determination by Multiple Foil Activation Iterative Method," *AWRL-TR-67-41*, Vol 1-4.

Nath, R., Meigooni, C., King, C., Smolen, S., d'Errico, F., 1993, "Superheated Drop Detector for Determination of Neutron Dose Equivalent to Patients Undergoing High-Energy X-Ray and Electron Radiotherapy," *Medical Physics* 20:78.

Nigg, D.W., 1994, "Methods for Radiation Dose Distribution Analysis and Treatment Planning in Boron Neutron Capture Therapy," *Int. J. Radiation Oncology Biol. Phys*., 28:1121-1134.

Nigg, D.W., Wheeler, F.J., Wessol, D.E., Capala, J., Chadha, M., 1997, "Computational Dosimetry and Treatment Planning for Boron Neutron Capture Therapy of Glioblastoma Multiforme," *Journal of Neuro-Oncology*, 33:93-104.

Nigg, D.W., Wemple, C.A., Wessol, D.E., Wheeler, F.J., 1999a, "SERA - An Advanced Treatment Planning System for Neutron Therapy and BNCT," *Trans. ANS, Bio. Med. Div.,* 80:66-68.

Nigg, D.W., Harker, Y.D., Hartwell, J.K., Wemple, C.A., Seren, T., Auterinen, I., Kotiluoto, P., Seppälä, T., Kortesniemi, M., Savolainen, S., Risler, R., 1999b, "Collaborative Neutronic Performance Characterization of the FiR 1 Clinical Epithermal Neutron Beam Facility for BNCT," In: Venhuizen, J.R. (ed.), *INEEL BNCT Research Program Annual Report – 1998*, INEEL-EXT-99-00293.

D.W. Nigg, C.A. Wemple, R. Risler, J.K. Hartwell, Y.D. Harker, G.E. Laramore, 2000, "Modification of the University of Washington Neutron Radiotherapy Facility for Optimization of Neutron Capture Enhanced Fast-Neutron Therapy," *Medical Physics* 27:359-367.

Nigg, D.W., Wemple, C.A., Seren, T., Seppälä, T., Auterinen, I., 2001, "Improved Evaluation of the Free-Beam Spectrum of the FiR 1 Clinical Epithermal Neutron Beam Facility for BNCT," In: Venhuizen, J.R. (ed.), *INEEL BNCT Research Program Annual Report – 2000*, INEEL-EXT-01-00204.

Nigg, D.W., Wemple, C.A., Venhuizen, J.R., Tripard, G.E., Sharp, S., Fox, K., Gavin, P.R., Sweet, V., 2002, Initial Performance Assessment of an Epithermal Neutron Beam for Neutron Capture Therapy Research at Washington State University," *Trans. ANS*, 87:397-398.

Nigg, D.W., 2003, "Computational Dosimetry and Treatment Planning Considerations for Neutron Capture Therapy," *Journal of Neuro Oncology*, 62:75-86.

Rhoades, W.A., et al., 1993, "TORT-DORT: Two and Three-Dimensional Discrete-Ordinates Transport," *Radiation Shielding Information Center, Oak Ridge National Laboratory*, CCC-543.

Roussin, R.W., 1980, "BUGLE-80 Coupled 47-Neutron, 20 Gamma-Ray P3 Cross Section Library," *Radiation Shielding Information Center, Oak Ridge National Laboratory,* DLC-75.

Venhuizen, J.R., et al., 2001, "Construction Progress of an Epithermal Neutron Beam for Preclinical BNCT Research at Washington State University," In: J.R. Venhuizen (ed.), *INEEL BNCT Research Program Annual Report – 2000*, INEEL-EXT-01-00204.

Venhuizen, J.R., et al., 2002, "Construction of an Epithermal Neutron Beam for Preclinical BNCT Research at Washington State University," In: J.R. Venhuizen (ed.), *INEEL BNCT Research Program Annual Report – 2001*, INEEL-EXT-02-00060.

Venhuizen, J.R., et al., 2003, "Neutronic Performance Assessment of an Epithermal Neutron Beam for Preclinical BNCT Research at Washington State University," In: J.R. Venhuizen (ed.), *INEEL BNCT Research Program Annual Report – 2002*, INEEL-EXT-03-00222.

Wheeler, F.J. and Nigg, D.W., 1994, *Feasibility Study for an Epithermal-Neutron Beam Facility at the Washington State University Radiation Center*, EGG-NRE-11296, Idaho National Engineering Laboratory, USA

Whittemore, W.L., 1992, "A Compact TRIGA Reactor for Boron Neutron Capture Therapy," In: Allen, B.J., et al. (ed), *Progress in Neutron Capture Therapy for Cancer,* Plenum Press, New York.

PROGRESS ON MEASUREMENT OF TRANSPORT BENCHMARKS FOR PHYSICAL DOSIMETRY TO SUPPORT DEVELOPMENT OF FAST-NEUTRON THERAPY WITH NEUTRON CAPTURE AUGMENTATION

D.W. Nigg[1], J.K. Hartwell[1], C.A. Wemple[1], R.Risler[2], G.E, Laramore[2], W. Sauerwein[3], G. Hüdepohl[3], A. Lennox[4]

1. Idaho National Laboratory, Idaho Falls, ID, USA
2. University of Washington Medical Center, Seattle, WA, USA
3. Universitatsklinicum Essen, Essen, Germany
4. Fermi National Accelerator Laboratory, Batavia, IL, USA

INTRODUCTION

The Idaho National Laboratory (INL), the University of Washington (UW) Medical Center, the University of Essen (Germany) Neutron Therapy Clinic, and the Northern Illinois University (NIU) Institute for Neutron Therapy at the Fermi National Accelerator Center (Fermilab) have been collaborating on efforts directed toward the development of supporting technologies required for advanced studies of fast-neutron therapy (FNT) with concurrent neutron capture (NCT) augmentation (Laramore et al. 1994). In addition to the development of optimized neutron sources (Nigg et al. 2000), UW, Essen, Fermilab and INL researchers are conducting measurements to produce suitable benchmark neutron dosimetry data for validation of advanced three-dimensional treatment planning methodologies required for successful administration of FNT/NCT.

This experimental effort has included several related components. Free-beam spectral measurements as well as phantom measurements with Lucite[a] cylinders using resonance and threshold activation foil techniques have now been completed at all three facilities. The same protocol was used for all measurements to facilitate inter-comparison of facilities. The activation results will be useful as a database for further detailed characterization of the neutron beams of interest as well as for validation of various explicit neutron transport codes and methodologies for FNT/NCT computational dosimetry, such as MCNP (Breismeister 2000), SERA (Nigg et al. 1999), and MINERVA (Nigg 2003).

METHODS AND MATERIALS

To illustrate the types of measurements that have been done, Figure 1 shows the UW treatment gantry, with the larger of the two Lucite phantoms in position on the patient couch. This phantom has a diameter of 15.2 cm and a height of 21.6 cm. The smaller phantom has corresponding dimensions of 12.7 x 18.2 cm. The isocenter of the beam was located at the center of the top phantom surface.

[a] Lucite is a registered trademark of E.I. du Pont de Nemours and Company

Figure 1. UW neutron therapy treatment facility with the large cylindrical Lucite phantom in position.

The field size at the isocenter was set to 7.8 cm x 8.0 cm for all irradiations. The measurements presented here are for the case with the UW "standard" beryllium neutron production target mounted in the gantry. The proton beam current incident on the target from the UW cyclotron in the adjacent room behind the gantry was 67 microamperes, with nominal proton energy of 50.5 MeV. Several different types of foil packages containing gold, manganese, aluminum, copper, and indium foils, with and without cadmium covers, were placed at various depths along the central axis of each phantom. The irradiation time in each case was generally one hour. After the completion of each irradiation, the induced activities resulting from the various interactions of interest in the foils were measured by gamma-ray spectrometry, and the results were converted to saturation activities or, equivalently, activation rates per atom per microampere of proton current impinging on the neutron production target during the irradiation. Free-beam spectral measurements have also been completed using various foil packages placed at the beam isocenter.

Figure 2 shows the fixed horizontal neutron beam facility at UW. The treatment head for the horizontal beam is of essentially the same design as the gantry-mounted treatment head. The proton beam from the UW cyclotron can be redirected to the horizontal head by a system of magnets. The horizontal beam is used primarily for physics measurements and other non-clinical applications. A specialized neutron production target, optimized for FNT/NCT applications (Nigg et al. 2000) was mounted in this treatment head, and all measurements performed for the gantry beam were repeated for the horizontal beam. This will provide a detailed comparison of the performance of the FNT/NCT neutron production target relative to that of the standard target.

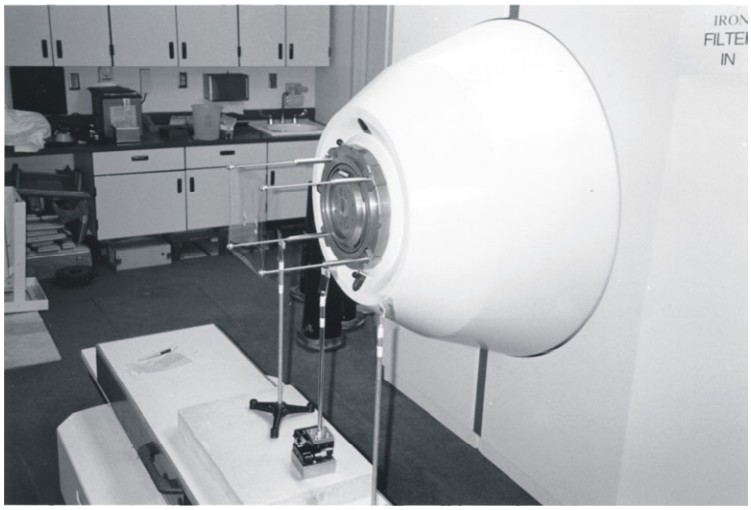

Figure 2. Horizontal neutron beam facility at the UW.

Figure 3 shows the Essen treatment gantry, with the larger phantom in place. Once again, the various measurements were repeated using the same protocol as was used for the UW measurements. The results will allow a direct inter-comparison of the performance of the Essen beam (which is produced by a deuteron beam incident on a beryllium target) relative to that of the two UW beams.

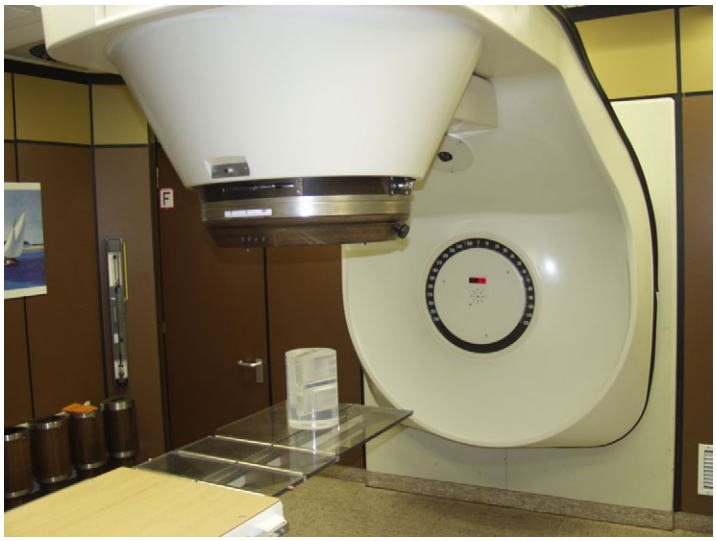

Figure 3. University of Essen Neutron Radiotherapy Facility with INL phantom.

Figure 4 shows a view of the exit port of the Fermilab facility, once again with the larger of the two phantoms in place. This facility features a fixed beam, with a somewhat higher energy neutron spectrum produced by 66 MeV protons impinging on a beryllium target. Patient positioning is accomplished by a chair that has the capability of precise rotation and translation to produce essentially any beam-patient orientation desired.

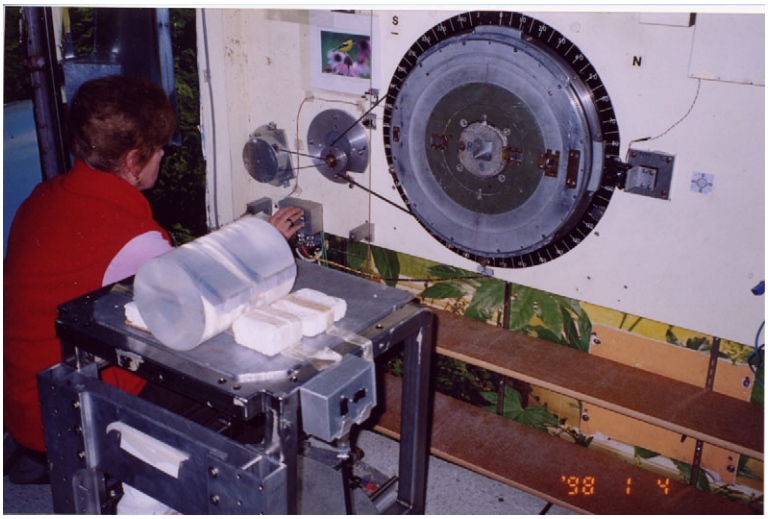

Figure 4. Neutron therapy facility at the Fermi National Accelerator Laboratory

RESULTS AND DISCUSSION

Figure 5 shows some typical results for the two phantoms in the UW gantry beam, as an illustration of the type of data that is of interest in the overall program. Analysis of data from all facilities will continue through FY 2005. In the case selected for presentation here, the activation of manganese with and without cadmium covers is shown as a function of depth in each phantom. In the case of the bare foils, most of the activation is due to thermal neutron absorption, and it can be seen that the thermal flux-depth curve is flatter for the larger phantom. This is as expected, since this phantom is more effective at thermalizing the higher-energy neutrons in the beam. However, with cadmium covers on the dosimeter packages, the activation is largely due to resonance neutron absorption at the primary resonance energy (340 eV) and above in both phantoms, and the curves are basically the same.

This information, along with information from the numerous other resonance and threshold interactions in the other foils, allows the development of a self-consistent picture of the space and energy dependent behavior of the neutron flux within the two phantoms. This, in turn, will provide benchmark data for validation of neutron transport computations required for beam characterization and treatment planning. Inter-comparison of the performance of the neutron beams at the three facilities on a common basis will also be facilitated.

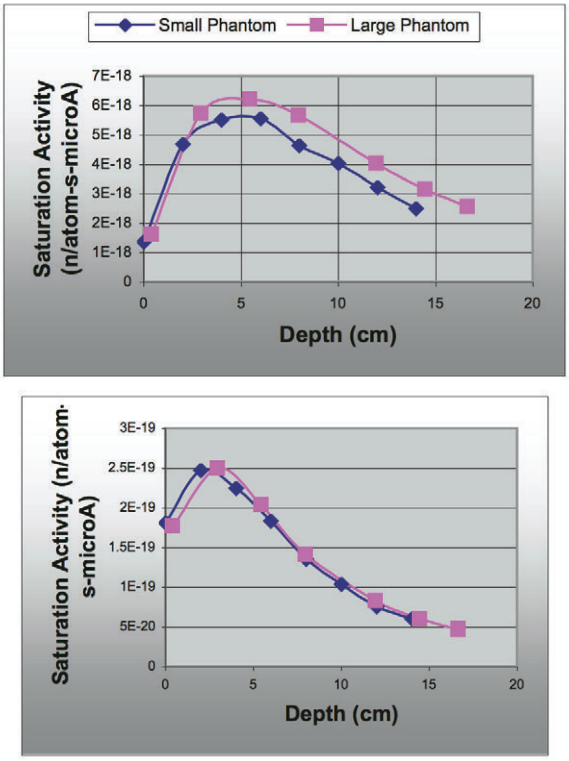

Figure 5. Saturation activities for Mn-56 in the small and large phantoms in the UW gantry beam, without (left) and with (right) cadmium foil covers. Uncertainties are comparable to the size of the data points shown.

REFERENCES

Laramore, G.E., Wootton, P., Livesey, J.C., Wilbur, D.S., Risler, R., Phillips, M., Jacky, J., Bucholtz, T.A., Griffin, T.W., Brossard, S., 1994, "Boron neutron Capture therapy - A mechanism for achieving a concomitant tumor boost in fast neutron radiotherapy," *Int. J. Rad. Onc. Bio. Phys*., 28:1135-1142.

D.W. Nigg, C.A. Wemple, R. Risler, J.K. Hartwell, Y.D. Harker, G.E. Laramore, 2000, "Modification of the University of Washington Neutron Radiotherapy Facility for Optimization of Neutron Capture Enhanced Fast-Neutron Therapy," *Medical Physics,* 27:359-367.

J.F. Breismeister, 2000, *MCNP – A General Monte Carlo N-Particle Transport Code, Version 4C*, LA-13709-M, Los Alamos National Laboratory, USA.

D.W. Nigg, C.A. Wemple, D.E. Wessol, F.J. Wheeler, 1999, "SERA-An Advanced Treatment Planning System for Neutron Therapy and BNCT," *Trans. ANS*, 80:66-68.

D.W. Nigg, 2003, "Computational Dosimetry and Treatment Planning Considerations for Neutron Capture Therapy," *J. Neuro Oncology,* 62:75-86.

COLLABORATIVE PHYSICAL AND BIOLOGICAL DOSIMETRY STUDIES FOR NEUTRON CAPTURE THERAPY AT THE RA-1 RESEARCH REACTOR FACILITY

D.W. Nigg[1], A.E. Schwint[2], J.K. Hartwell[1], E.M. Heber[2], V. Trivillin[2], J. Castillo[2], L. Wentzeis[2], P.E. Sloan[3], C.A. Wemple[1]

1. Idaho National Laboratory, Idaho Falls, ID, USA
2. Comisión Nacional de Energía Atómica, Centro Atómico Constituyentes, Buenos Aires, Argentina
3. University of Illinois, Champaign-Urbana, Illinois, USA

INTRODUCTION

The National Atomic Energy Commission of Argentina (CNEA) has constructed a thermal neutron source for possible use in Boron Neutron Capture Therapy (BNCT) applications at the RA-1 research reactor facility located in Buenos Aires, Argentina. The Idaho National Laboratory (INL) and CNEA, under a bilateral U.S./Argentina agreement on peaceful uses of nuclear science, have jointly conducted some basic physical dosimetric characterization measurements and some limited small-animal radiobiological dose ranging studies focused on investigation of the potential utility of this neutron source for neutron capture therapy preclinical research applications. The experimental protocol for the physical dosimetry included several sets of standard activation measurements to characterize the neutron spectrum and dose parameters at the irradiation location, as well as a set of thermoluminescent dosimeter (TLD) measurements to characterize the gamma field. The radiobiological studies employed a hamster cheek pouch oral cancer model validated for BNCT studies by CNEA using an alternate, hyperthermal neutron source available at the RA-6 research reactor in San Carlos de Bariloche, Argentina (Trivillin et al. 2004; Kreimann et al. 2004). The work presented here has been motivated by the fact that the RA-1 facility is co-located with the CNEA radiobiological research laboratories in Buenos Aires, thereby offering some potential advantages in terms of geographical convenience, cost, and research productivity.

DESCRIPTION OF THE RA-1 FACILITY

The RA-1 reactor, with a rated operating power of 40 kilowatts, is of the open-tank type with an enriched uranium (20% ^{235}U) oxide annular core, moderated and cooled by demineralized light water, and reflected internally and externally by graphite. The core is formed by 228 cylindrical fuel rods distributed in five concentric circles as shown in Figure 1. The outside diameter of the core is 335 mm and the inside diameter is 153 mm. Each fuel element is composed of a 540 mm UO_2 active axial length fuel segment with a 60mm graphite reflector segment on each end. All three axial segments are encapsulated in 1 mm thick aluminum cladding with an outside diameter of 10 mm.

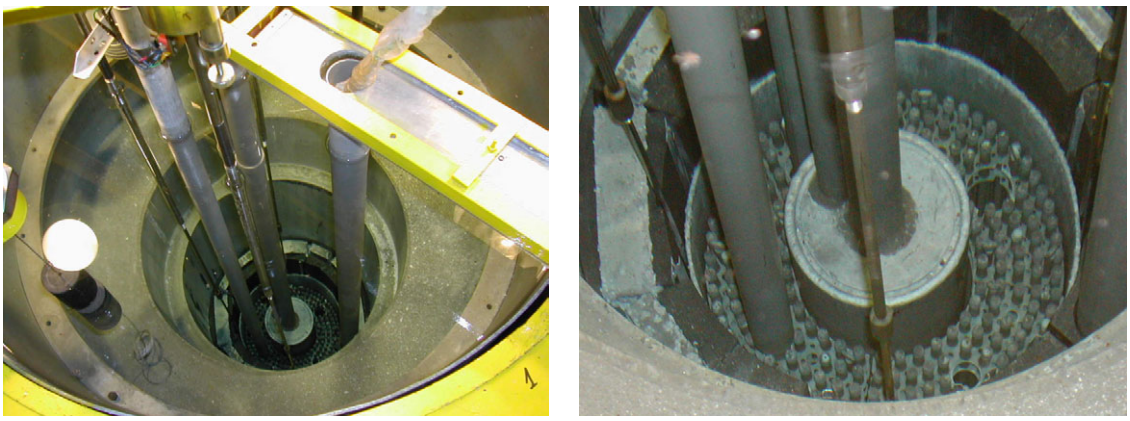

Figure 1. View into the RA-1 tank from the top showing the annular lattice of water-moderated fuel elements.

The reactor is controlled by means of four cadmium rods encapsulated in stainless steel, located between the core and the external reflector, azimuthally separated from each other by 90 degrees. The control rods are coupled by electromagnets to drive mechanisms located in the metal structure above the tank. The drive mechanisms are powered by stepper motors operated from the control room. A set of sensors constantly transmits the exact position of each rod.

A transverse sectional view of the reactor and the adjacent graphite thermal column and shielding structure is shown in Figure 2. To produce the irradiation configuration, a cavity was made in the previous solid graphite thermal column as shown. This allowed an irradiation position closer to the reactor core, increasing the neutron flux compared to the case with the full-thickness thermal column (1600 mm), albeit at the cost of some decrease in the thermal nature of the spectrum that is produced. A small cart moves in and out of the cavity, using a system of tracks and pulleys to position the experimental animals at the irradiation point. This cart is shown in Figure 3. A "shielding box" constructed from two plates of Lucite[a] with 6 mm of enriched lithium carbonate sandwiched between them is mounted on hinges connected to the bed of the cart. The cart is moved into the cavity with the shielding box in the folded position. The box is then rotated upright on the hinges to position the experimental animals for irradiation.

Figure 4 shows how the experimental animals are positioned in the shielding box, which is designed for irradiation of two animals at a time. A Lucite hamster phantom is shown in one of the two available positions. In the case of an actual hamster, the cheek pouch, i.e. either a normal non-cancerized pouch or a tumor-bearing cancerized pouch, is everted and spread on the flat surface to the animal's right. A lithium-Lucite cover plate is then placed over the hamster. The arrangement allows the cheek pouch to be exposed to essentially the full thermal flux field at the irradiation point while reducing the thermal neutron flux in the main body of the hamster via thermal neutron capture in the surrounding ^{6}Li, which captures thermal neutrons without producing secondary gammas.

[a] Lucite is a registered trade mark of E.I. du Pont de Nemours and Company

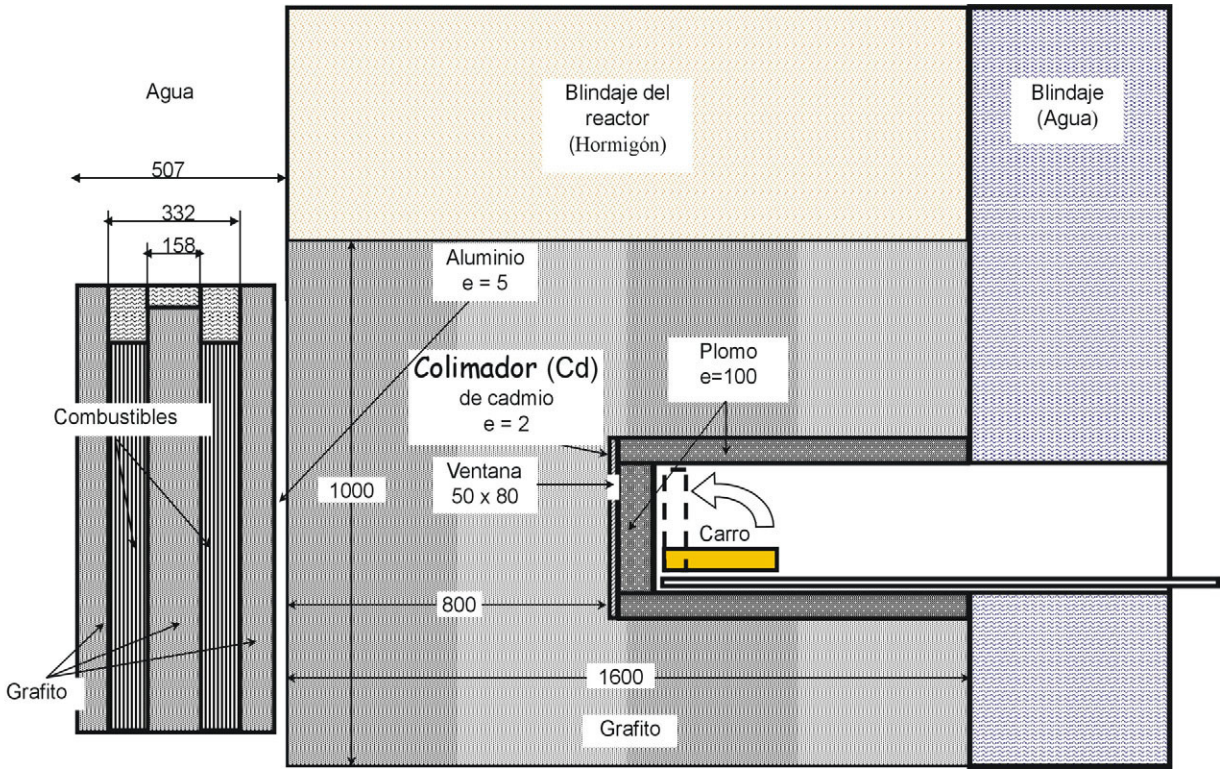

Figure 2. Transverse section of the RA-1 reactor and adjacent thermal column, taken through the core centerline. (Note: Carro = cart, Combustibles = Fuel Elements, Blindaje = Shielding, Hormigon = Concrete, Agua = Water, Plomo = Lead, Grafito = Graphite, Colimador = Collimator, Ventana = Window, e = espesor = thickness. All dimensions are in mm).

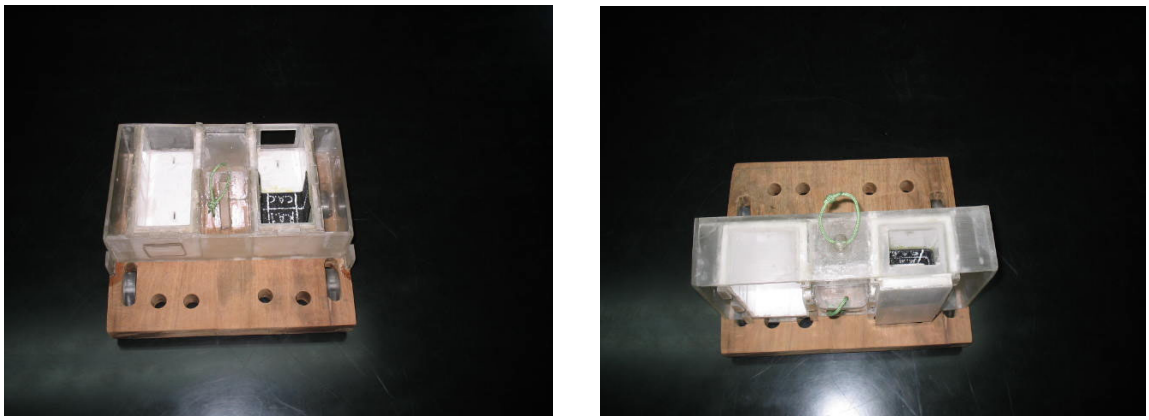

Figure 3. Irradiation cart with lithium carbonate lined shielding box in the folded (left) and upright (right) positions.

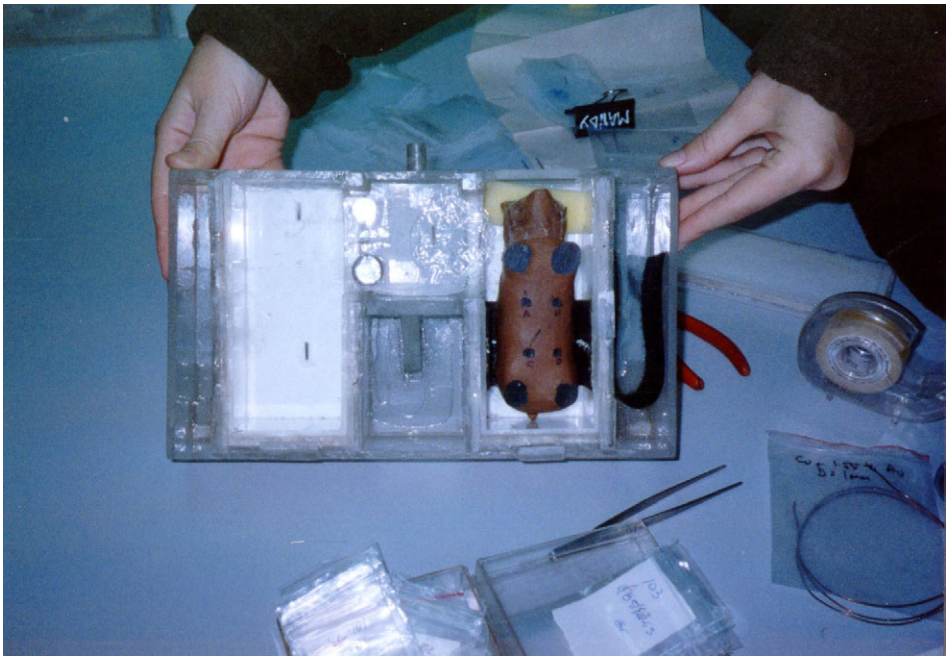

Figure 4. Shielding box with hamster phantom in position, prior to placement of lid.

Figure 5 shows the assembled cart and shielding box positioned at the entrance to the irradiation cavity in the thermal column. Figure 6 shows a view into the cavity with the cart in the irradiation position prior to rotation of the shield box. Irradiations are conducted by bringing the reactor to its rated power of 40 kW, sliding the cart into position to begin the irradiation, and then withdrawing it to end the irradiation after the desired time has elapsed.

Figure 5. Irradiation cart with assembled shielding box, positioned at the entry to the thermal column.

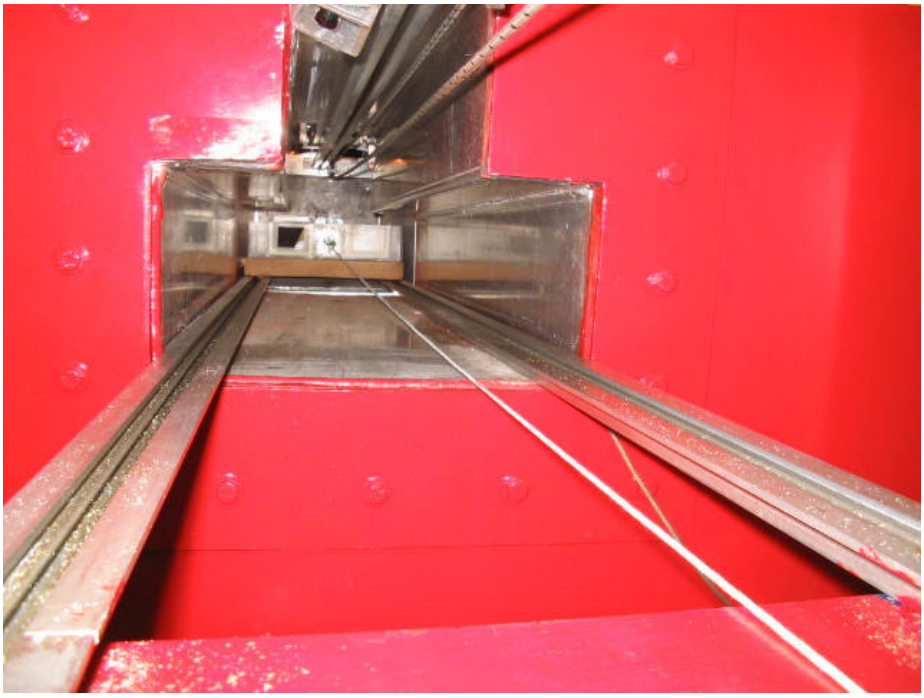

Figure 6. View into the thermal column penetration showing the irradiation cart in position at the irradiation point prior to rotation of the shield box into the upright position.

PHYSICAL DOSIMETRY

The neutron field characterization measurements were performed using simplified extensions of neutron activation analysis techniques (Nigg et al. 1999; Harker et al. 1992) that have been adapted for BNCT applications by the INL through extensive experience with several other medical neutron facilities in the U.S. and in Europe. Gamma field measurements were conducted using standard TLDs. Auxiliary neutron transport computations of various types are also required as part of the experimental protocol. The various computational and experimental methods used for the RA-1 source characterization are described in the following sections.

Computational Methods

The *a-priori* spectrum produced by the RA-1 facility at the irradiation location was computed using the well-known DORT discrete-ordinates transport code (Rhoades and Childs 1982) with the BUGLE-80 47-group neutron cross-section library (Roussin 1980). The reactor and thermal column arrangement shown in Figure 2 was approximately modeled in two-dimensional cylindrical geometry with the z-axis coinciding with the axis of neutron flow from the reactor, through the graphite thermalization region and into the irradiation cavity, i.e., from left to right in Figure 2. This required approximating the reactor core as a cylinder on its side, but experience has shown that this approximation is appropriate, provided key region volumes, core reactivity, and key region thicknesses along the axis of neutron flow are preserved. Additional calculations to determine spectrum unfolding parameters for the activation measurements were performed using the

computed flux taken from the DORT model at a transverse plane just upstream of the irradiation point, coupled with an MCNP (Breismeister 2000) Monte Carlo transport model of the activation foil and wire packages.

Activation Foil Measurements in the Free Beam

Activation measurements to characterize the free-field neutron source were conducted using neutronically thick circular foils of various types. The foil specifications and corresponding neutron activation interactions of interest are listed in Table 1. Because of the limited time available, a very simple set of foils was used for these measurements. Nonetheless, useful results were still obtained.

The basic experimental arrangement for positioning the foils in the beam is shown in Figure 4. Standard 12.7-mm (0.5 inch) diameter gold, copper, tungsten, and indium foils were placed in the irradiation position occupied by the everted hamster cheek pouch on the outer surface of the shielding box. A cadmium cover was placed around this set of foils to suppress the thermal-neutron response. Each cadmium-covered foil thus responds largely to neutrons having energies at or near the energy of the respective primary resonance of the foil material, as shown in Table 1. Uncovered gold and manganese foils were also placed in the irradiation position to permit a measurement of the thermal flux. The foils had nominal thicknesses in the range of 0.0254 mm (0.001 inch) to 0.127 mm (0.005 inch), depending on the material type.

Table 1. Activation interactions and foils used in the INL/CNEA measurements.

Neutron Interaction	Energy Range of Primary Response	Activation Gamma Energy of Interest (keV)
^{55}Mn (n, σ) Bare Foil	Thermal	847
^{197}Au (n, σ) Bare Foil	Thermal	411
^{115}In (n, σ) Cd Cover	1 eV Resonance	1293,1097, and 416
^{197}Au (n, σ) Cd Cover	5 eV Resonance	411
^{186}W (n, σ) Cd Cover	18 eV Resonance	686
^{63}Cu (n, σ) Cd Cover	1 keV Resonance	511 (Positron)
^{115}In (n, n') Cd Cover	430 keV Threshold	336

The cadmium covered indium foil was also used to provide additional spectral information in the energy range above epithermal (> 10 keV). In addition to the prominent gamma lines from ^{116}In that result from neutron capture in ^{115}In, there is also a relatively weak 336 keV gamma line from an isomer of ^{115}In that is formed by inelastic scatter. This latter interaction can be used to gauge the neutron flux above the threshold for this interaction (~400 keV).

Use of the foils as described provided 7 basic neutron response functions having a useful degree of linear independence. These response functions were:

1. Resonance capture in the copper, tungsten, gold, and indium foils, all with thermal neutron capture suppressed by cadmium (4 responses);
2. Total neutron capture in the uncovered gold and manganese foils (2 responses);
3. Inelastic scatter in the cadmium covered indium foil (1 response).

The measurements reported here are based on the results of a one-hour irradiation at a reactor power of 40 kW.

The irradiated foils were assayed using an Ortec gamma spectrometer system recently placed into operation at the CNEA reactor laboratory. The system consisted of an high-purity germanium (HPGe) detector and a a DigiDart™ digital gamma ray spectrometer, coupled with the Gamma Vision™ data acquisition and analysis software. This detector system was calibrated for energy and efficiency using standard traceable sealed gamma sources available at the CNEA laboratory. The final measured saturation activities for the foils are presented in Table 2. Some additional independent measurements of the activation of cadmium-covered gold and indium foils and for a bare gold foil were performed by the CNEA staff separately from the collaborative measurements performed by INL personnel. The results of these measurements, also shown in Table 2, serve to help validate the larger set of measurements performed in the collaboration with INL.

Table 2. Saturation activities for the foils used in the RA-1 free beam spectrum measurements. Uncertainties are given in parentheses at the 1σ level.

Interaction Type	Measured Activation Rate per Atom (INL)	Measured Activation Rate per Atom (CNEA)
^{55}Mn (n, σ) Bare Foil	1.96×10^{-15} (3.0%)	
^{197}Au (n, σ) Bare Foil	1.86×10^{-14} (3.1%)	1.96×10^{-14} (10.0%)
^{115}In (n, σ) Cd Cover	9.60×10^{-15} (3.2%)	
^{197}Au (n, σ) Cd Cover	3.85×10^{-15} (3.1%)	3.53×10^{-15} (11.3%)
^{186}W (n, σ) Cd Cover	2.15×10^{-15} (6.4%)	
^{63}Cu (n, σ) Cd Cover	3.89×10^{-17} (6.6%)	
^{115}In (n, n') Cd Cover	3.93×10^{-18} (13.5%)	3.63×10^{-18} (8.3%)

Phantom Measurements

Measurements of the thermal and epithermal neutron distribution at various points on the surface of and within the Lucite hamster phantom were also conducted, primarily to estimate the effect of placing the hamster in the shielding box, which was designed to reduce the thermal neutron flux in the main body of the hamster relative to that seen by the everted cheek pouch on the outer surface of the box, as discussed previously. Figure 4 shows the hamster phantom in position – in an actual animal irradiation the cheek pouch would be everted to expose the tumors and extended to the hamster's right in the photo, with the tumor region placed roughly at the location of the flux wire that can be seen to the right of the phantom in the photo. The flux wires used for the measurements reported here were approximately 8 mm in length and 1 mm in diameter. Each wire had

a mass of approximately 70 mg, and was composed of copper alloyed with 1.55 percent gold by weight. This provided two linearly-independent activation responses (neutron absorption in Cu-63 and Au-197) that were used to estimate the flux distribution in and around the hamster phantom. The activation responses of the wires could also be used to unfold a two-group (thermal and above-thermal) neutron spectrum at each flux wire location, but this was not done in the work presented here. Wires were placed at the irradiation location where the everted cheek pouch would be, as well as in holes drilled at various points throughout the phantom head and body, and at various locations on the hamster surface. There were 15 wires in total.

Spectral Unfolding Procedure

The activation rates of the various foils and wires were used to estimate the neutron spectrum of the RA-1 beam and the fluxes in the water phantom by way of a direct least-squares unfolding procedure adapted by the INL for this type of measurement and documented in Nigg et al. (2000).

Results

Table 3 shows the results for a three-group (thermal, epithermal, and fast) neutron flux spectrum unfolded from the seven foil responses using the direct method described above. This particular three-group structure was selected for consistency with standard epithermal-neutron BNCT flux definition conventions. Three-group *a-priori* fluxes calculated by integration of the 47-group calculated *a-priori* flux spectrum over the energy ranges indicated are also shown. The unfolding procedure produces measured results that are significantly different from the *a-priori* flux. The measured fast and epithermal fluxes are considerably higher and the thermal flux is lower. The measured thermal flux is, however, consistent with independent results obtained earlier by CNEA using the gold activation rates shown in the right-hand column of Table 2 and with the Westcott theory (Westcott 1962) for estimating the flux from the saturation activity. The significant difference between the computed and measured fluxes in Table 3 indicates that the approximate models used in this work, while adequate to estimate unfolding parameters for the initial measurements of interest here, should be updated to represent the RA-1 system in more detail prior to being used for actual dosimetry and irradiation planning.

Background neutron dose rates and boron dose rates per ppm boron-10 are also shown in Table 3. These were computed by combining the measured flux results with kerma factors for standard tissue developed from the basic kerma data provided in File 27 of the BUGLE library. About 85% of the neutron background dose is from hydrogen recoil, and an additional 5% is from nitrogen capture. The remainder is from several minor components, primarily carbon and oxygen recoil. Finally, Table 3 includes the results of gamma dose measurements performed independently by CNEA using TLDs located in the everted pouch position on the shielding box.

Table 3. Calculated and measured integral flux parameters for the CNEA RA-1 thermal neutron source facility at the irradiation point outside of the lithium carbonate shield box. Uncertainties are given in parentheses at the 1σ level. The reactor power is 40 kW.

Quantity	*A-Priori* Calculation	Direct Unfolding	Iterative Adjustment
Fast Neutron Flux 10 keV < E < 17.33 MeV (n/cm^2-sec)	3.80×10^6	4.72×10^7 (19.5%)	3.01×10^7
Epithermal Neutron Flux 0.404 eV < E < 10 keV (n/cm^2-sec)	1.36×10^7	5.28×10^7 (11.5%)	5.63×10^7
Thermal Neutron Flux E < 0.414 eV (n/cm^2-sec)	2.34×10^8	1.51×10^8 (3.7%)	1.83×10^8
Neutron Dose Rate (cGy/min)	0.569	6.97	4.47
Boron Dose Rate (cGy/min-ppm ^{10}B)	9.34×10^{-2}	6.03×10^{-2}	7.31×10^{-2}
Gamma Dose Rate CNEA TLD Measurement (cGy/min)	N/A	1.3	1.3

Figure 7 shows the results of an alternate spectrum estimation procedure based on adjusting the 47-group *a-priori* neutron spectrum using an INL implementation of an iterative adjustment method described by Draper (Draper 1971). This method is a variation of the approach used in the well-known SAND-II code (McElroy et al. 1967). It attempts to find a spectrum that reproduces the measured foil responses as closely as possible by iteratively adjusting the *a-priori* fine group flux until a satisfactory result is obtained, as indicated by the behavior of the reduced chi-squared parameter for the fit and by the absence of further significant change in the adjusted spectrum from one iteration to the next. During each iteration through the energy groups, the adjustment factor for the flux in a given group is taken as the weighted sum of the ratios determined by dividing the measured reaction rate by the computed reaction rate for each foil response, where the calculated reaction rate for each response is computed using the flux spectrum from the previous iteration. The weight function is simply the macroscopic activation cross section for each foil in each group. Typically, only a few iterations through the energy groups are required to produce a reasonable result using this method. The *a-priori* and adjusted fluxes for the RA-1 neutron source are shown in Figure 7. Once again, the fast flux is increased considerably by the adjustment procedure, analogous to the results of the direct unfolding method. Integrals of the adjusted fluxes over the energy ranges for the three-group structure are also included in Table 3. These are reasonably consistent with the direct unfolding results, although the fast flux is somewhat lower. This discrepancy is believed to be attributable to high statistical uncertainties in the fine-group *a-priori* fast-neutron flux spectrum. These uncertainties

are reduced considerably when the three-group flux unfolding parameters are produced for the direct unfolding method by coalescing the fine-group fluxes. As a result, experience has shown that the direct unfolding results generally can be assumed more accurate if there are discrepancies of this type.

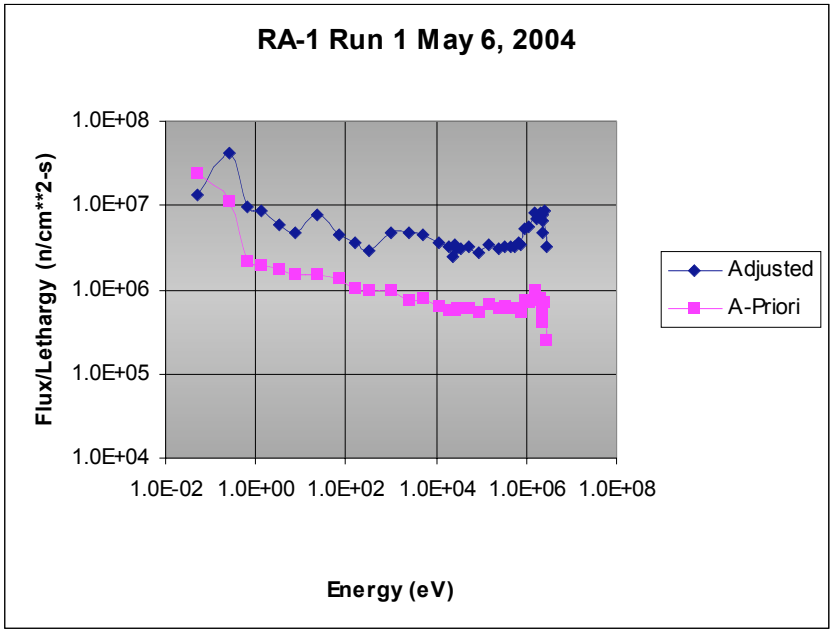

Figure 7. Unfolded free beam neutron spectrum obtained by iterative adjustment for the CNEA RA-1 thermal neutron source facility. The reactor power is 40 kW.

It is also possible to validate the directly-unfolded fast-neutron flux by further examining the activation rate of the isomeric state of ^{115}In. Recall that the inelastic scattering interaction that leads to this state, which decays with the emission of a 336 keV gamma, has a threshold in the range of 400 keV. Thus, the inelastic scatter interaction rate that is measured is a direct indicator of the neutron flux above this energy. The two independent measurements of this interaction rate (Table 2) give very consistent results for RA-1, roughly 3.75 x 10^{-18} interactions/atom-s.

With regard to the phantom measurements, no fluxes were unfolded from the flux wire activation rates because of the lack of adequate computational models to compute the required parameters at this stage of the project. However, based on the copper activation rates measured for the wires it can be estimated that the thermal flux in the parts of the hamster body that are protected by the lithium shield is in the range of 20-40% of what it is at the unprotected everted pouch position. This appears consistent with the TLD gamma measurements performed by CNEA. The gamma dose measured for the parts of the hamster body protected by the shield was generally about half of that measured for the everted pouch position. This indicates a reduction in the hydrogen capture gamma dose rate (proportional to the thermal neutron flux) in the protected regions of the phantom. The reduction is less than for the thermal flux itself because there is also a

constant background gamma dose throughout the phantom inside and outside of the shield box from the incident gamma field from the reactor as well as from capture gammas in the cadmium and lead shielding in the irradiation cavity.

Using the data from Table 3, one can estimate the total physical (i.e., unweighted) dose at the irradiation location for a hypothetical, but realistic, case where there is 50 ppm in the irradiated tissue as follows:

Background Neutron Dose:	6.97 cGy/min (all sources)
Gamma Dose:	1.30 cGy/min (capture + incident)
Boron Dose	3.02 cGy/min
Total	11.29 cGy/min

Thus the background neutron dose is over half of the total and the selective boron dose is only about 25% of the total in this case. Changes in the RA-1 beam design that are currently underway will permit a significant improvement in the neutron spectrum.

BIOLOGICAL DOSIMETRY

The radiobiological dose ranging studies involved two types of hamster irradiations. The first was a limited set of irradiations using the RA-1 neutron source without administration of a boron agent in order to gauge the background dose from the mixed neutron-gamma field at the irradiation location. Additionally, a few initial irradiations were performed using boronated phenylalanine (BPA) as well as a potential alternate agent for BNCT. This alternate agent, GB-10 ($Na_2B_{10}H_{10}$), may offer some advantages (Heber et al. 2004), either alone or in combination with the more commonly used BPA. GB-10 is not new, but interest in its possible use has re-emerged recently because of its biochemical performance and the development by INL of an improved synthesis technique for the key precursor, decaborane. GB-10 is a diffusive agent that has been shown to achieve high (~100 ppm) blood-boron concentrations in human biodistribution studies without toxicity. This is an improvement over the performance of the other largely diffusive agent that is currently approved for human studies, borocaptate sodium, or BSH. Although a large macroscopic tumor/blood differential would not be expected with GB-10, it may be that microscopic distributions of GB-10 in and around tumor cells would be more uniform than appears to be the case with BPA. BPA, commonly used in human NCT trials worldwide, is an active agent that achieves, at least on a macroscopic scale, a significant tumor/blood differential uptake ratio, but there are questions about whether the microscopic (cell to cell) distribution is sufficiently uniform to provide adequate coverage of the target cells. Hypothetically, if GB-10 were administered in combination with BPA, macroscopic selectivity would be traded against microscopic uniformity in order to obtain an improved overall optimum coverage of tumor cells. This means that fewer cells are left with a non-therapeutic level of boron, and potentially also offers additional mechanisms for tumor control. This hypothesis has been the subject of the ongoing INL/CNEA collaboration using the RA-6 neutron beam. The study presented here is intended to gauge the feasibility of extending this collaboration to irradiations using the RA-1 facility.

The hamster cheek pouch oral cancer model has been validated for BNCT studies as noted previously. Successful tumor control and the absence of normal tissue radiotoxicity have been evidenced by performing *in-vivo* BNCT mediated by GB-10, and GB-10 and BPA administered jointly (Trivillin et al. 2004), and BNCT mediated by BPA alone (Kreimann et al. 2004) using the RA-6 hyperthermal neutron beam. Within this context, both normal tissue response and tumor control have been extensively characterized. Thus, the response of the hamster cheek pouch oral cancer model for different exposure times and irradiation conditions at RA-1 was able to be accessed for contributions to the characterization of this beam in terms of radiobiological parameters.

The first set of irradiations at RA-1 involved no body shielding and short (10 minutes) exposures. Six normal hamsters (non-cancerized) were irradiated with beam only, nine normal hamsters were treated with BPA-BNCT (15.5 mg ^{10}B/kg body weight) and nine normal hamsters were treated with GB-10-BNCT (50 mg ^{10}B/kg body weight). The response of normal, non-cancerized animals is clinically relevant in terms of assessing potential radiotoxicity in dose-limiting tissues in animals that will survive long enough to show long-term effects. Macroscopic analysis and histological evaluation revealed no radiotoxic effects up to the last experimental time-point evaluated (3 months).

Eight cancerized hamsters bearing 12 tumors were then treated with BPA-BNCT (15.5 mg ^{10}B/kg body weight) and a 10 minute exposure time, and they exhibited 50% tumor control (complete remission + partial remission) by 2 weeks post-treatment with no radiotoxic effects. Three cancerized hamsters bearing 5 tumors were treated with GB-10-BNCT (50 mg ^{10}B/kg body weight) and a 10 minute exposure time, and they exhibited 60% tumor control by 2 weeks post-treatment with no radiotoxic effects. These irradiations revealed that 10 minute exposures resulted in no radiotoxicity, even with whole body exposure to the beam, coupled with significant tumor control.

The second set of irradiations involved the use of the body shielding box described above, as well as longer exposure times to examine the degree of protection conferred by the shielding device, the maximum tolerated exposure time, and the potential tumor control associated to the varying degrees of radiotoxicity. Four normal hamsters were irradiated with beam only for 45 minutes and one normal hamster was irradiated with beam only for 60 minutes. All five hamsters have failed to show radiotoxic effects up to 3-5 months post-irradiation, the last experimental times evaluated. Three normal hamsters were irradiated with beam only for 75 minutes, and were sacrificed 9 days post-irradiation due to severe radiotoxicity. One normal hamster was treated with BPA-BNCT (15.5 mg ^{10}B/kg body weight) with an exposure time of 45 minutes, and has failed to show radiotoxic effects up to 3.5 months post-treatment, the last experimental time evaluated.

Two cancerized hamsters bearing 3 tumors were treated with GB-10-BNCT (50 mg ^{10}B/kg body weight) with an exposure time of 75 minutes. The animals died at 6 days post-treatment due to severe radiotoxicity, and exhibited 100% tumor control. Two hamsters bearing 10 tumors were treated similarly at an exposure time of 45 minutes. These animals died 6-21 days post-treatment due to severe radiotoxicity, and exhibited

90% tumor control. Two hamsters bearing 8 tumors were treated with BPA-BNCT (15.5 mg ^{10}B/kg body weight) with an exposure time of 45 minutes. Some signs of radiotoxicity were observed coupled with 100% tumor control. One hamster bearing two tumors was treated with GB-10-BNCT (50 mg ^{10}B/kg body weight) with an exposure time of 30 minutes. Thirty days post-treatment it had failed to exhibit radiointroduced toxicity, and had shown 50% tumor control. One hamster bearing 8 tumors was treated with BPA-BNCT (15.5 mg ^{10}B/kg body weight) with an exposure time of 30 minutes. The animal was sacrificed at 14 days post-treatment due to moderate radiotoxicity. Tumor control was 50% for this animal.

Despite the small sample assessed, these irradiations suggest that it would not be possible to perform BNCT mediated by GB-10 or BPA alone at exposure times in excess of 30 minutes without exceeding normal tissue tolerance at RA-1. Within the context of the data obtained in previous studies at RA-6, the fact that high tumor control is associated with unacceptable radiotoxicity would suggest a proportionally small boron dose component associated to excessive background dose at RA-1. The present radio-biological findings confirm that the background dose causing the radiotoxic effects observed herein would originate in the fast neutron/gamma dose components, rather than in the thermal neutron dose component for which the shielding would act as an effective protection.

The fact that BNCT mediated by the combined administration of GB-10 and BPA reduces the dose to normal tissue (Trivillin et al. 2004) is particularly interesting in scenarios such as RA-1 in which a reduction in background dose is particularly contributory. Within this context, further RA-1 optimization studies on BNCT mediated by GB-10 + BPA are warranted within the context of escalating the dose to tumor without exceeding normal tissue tolerance.

DISCUSSION

The RA-1 facility is the second neutron source specifically constructed for NCT research in Latin America, and one of only about 12 such facilities currently operational in the world. The results presented here provide an initial assessment of the performance of this neutron source using simple but reliable experimental techniques. The results show that the neutron flux intensity is sufficient for meaningful research applications, but that the spectrum is currently not optimal. However, improvements are underway that should increase the thermal neutron flux (and thus the selective boron dose component) relative to the background fast and epithermal neutron flux and the resulting nonselective background dose.

ACKNOWLEDGEMENTS
INL participation in this work was sponsored by the U.S. Department of Energy (DOE), Office of Nuclear Nonproliferation (NN-44), through the Sister Laboratory Program at the Argonne National Laboratory (ANL). The INL and CNEA participants would like to acknowledge the assistance and support of Dr. Basil Picologlou (ANL), Dr. Kirsten Laurin-Kovitz (ANL), Dr. Margaret Manning (DOE), and Dr. Sara Liberman (CNEA) in particular.

REFERENCES

Breismeister, J.F., 2000, *MCNP – A General Monte Carlo N-Particle Transport Code, Version 4C*, LA-13709-M, Los Alamos National Laboratory.

Draper, E.L. Jr., 1971, "Integral Reaction Rate Determinations – Part I: Tailored Reactor Spectrum Preparation and Measurement," *Nuclear Science and Engineering* 46:22-30.

Harker, Y.D., et al., 1992, "Spectral Characterization of the Epithermal Neutron Beam at the Brookhaven Medical Research Reactor," *Nuclear Science and Engineering*, 110:355-368.

Heber, E.M., Trivillin, V.A., Nigg, D.W., Kreimann, E.L., Itoiz, M.E., Rebagliati, R.J., Batistoni, D., Schwint, A.E., 2004, "Biodistribution of GB-10 Compound for Boron Neutron Capture Therapy (BNCT) in an Experimental Model of Oral Cancer in the Hamster Cheek Pouch," *Archives of Oral Biology,* 49:313-324.

Kreimann, E.L., Itoiz, M.E., Longhino, J., Blaumann, H., Calzetta, O., Schwint, A.E., 2004, "Boron Neutron Capture Therapy for the Treatment of Oral Cancer in the Hamster Cheek Pouch Model," *Cancer Research (Advances in Brief)*, 61: 8638-8642.

McElroy, W.N., et al., 1967, "SAND-II Neutron Flux Spectra Determination by Multiple Foil Activation Iterative Method," *AWRL-TR-67-41*, Vol 1-4.

Nigg, D.W., et al., 1999, "Collaborative Neutronic Performance Characterization of the FiR 1 Clinical Epithermal-Neutron Beam Facility for BNCT," In: J.R. Venhuizen (ed), *INEEL BNCT Research Program Annual Report 1998*, INEL/EXT-99-00293, April 1999, pp 13-38.

Nigg, D.W., Wemple, C.A., Risler, R., Hartwell, J.K., Harker, Y.D., Laramore, G.E., 2000, "Modification of the University of Washington Neutron Radiotherapy Facility for Optimization of Neutron Capture Enhanced Fast-Neutron Therapy," *Medical Physics*, 27:359-367.

Rhoades, W.A. and Childs, R.L., 1982, *An Updated Version of the DOT-4 One- and Two - Dimensional Neutron/Photon Transport Code*, ORNL-5851, Oak Ridge National Laboratory.

Roussin, R.W., 1980, "BUGLE-80 Coupled 47-Neutron, 20 Gamma-Ray P3 Cross Section Library," *Radiation Shielding Information Center, Oak Ridge National Laboratory,* DLC-75.

Trivillin, V.A., Heber, E.M., Itoiz, M.A., Nigg, D.W., Calzetta, O., Blaumann, H., Longhino, J., Schwint, A.E., 2004, "Radiobiology of BNCT Mediated by GB-10 and GB-10 + BPA in Experimental Oral Cancer," *Applied Radiation and Isotopes*, 61:939-945.

Westcott, C.H., 1962, *Effective Cross Section Values for Well-Moderated Thermal Reactor Spectra*, AECL-1101.